



UNIVERSITY OF LEEDS

This is a repository copy of *The turbulent burning velocity of methanol-air mixtures*.

White Rose Research Online URL for this paper:

<http://eprints.whiterose.ac.uk/78351/>

Article:

Vancoillie, J, Sharpe, G, Lawes, M et al. (1 more author) (2014) The turbulent burning velocity of methanol-air mixtures. *Fuel*, 130. 76 - 91. ISSN 0016-2361

<https://doi.org/10.1016/j.fuel.2014.04.003>

Reuse

Unless indicated otherwise, fulltext items are protected by copyright with all rights reserved. The copyright exception in section 29 of the Copyright, Designs and Patents Act 1988 allows the making of a single copy solely for the purpose of non-commercial research or private study within the limits of fair dealing. The publisher or other rights-holder may allow further reproduction and re-use of this version - refer to the White Rose Research Online record for this item. Where records identify the publisher as the copyright holder, users can verify any specific terms of use on the publisher's website.

Takedown

If you consider content in White Rose Research Online to be in breach of UK law, please notify us by emailing eprints@whiterose.ac.uk including the URL of the record and the reason for the withdrawal request.



eprints@whiterose.ac.uk
<https://eprints.whiterose.ac.uk/>

The turbulent burning velocity of methanol-air mixtures

J. Vancoillie^a, G. Sharpe^b, M. Lawes^b, S. Verhelst^a

^a*Department of Flow, Heat and Combustion Mechanics, Ghent University
Sint-Pietersnieuwstraat 41 B-9000 Gent, Belgium*

^b*School of Mechanical Engineering, University of Leeds
Leeds LS2 9JT, UK*

5

Abstract

Methanol is a sustainable and versatile alternative fuel for spark-ignition engines and other combustion applications. To characterize the combustion behavior of this fuel, a good understanding of the factors affecting its turbulent burning velocity is required. This paper presents experimental values of the turbulent burning velocity of methanol-air mixtures obtained in a fan-stirred bomb, for $u' = 2-6$ m/s, $\phi = 0.8-1.4$, $T = 358$ K and pressures up to 0.5 MPa. In combination with laminar burning velocity values previously obtained on the same rig, these measurements are used to provide better insight into the various factors affecting u_t of methanol, and to assess to what degree existing turbulent combustion models can reproduce experimental trends. It appeared that most models correctly accounted for the effects of turbulent rms velocity u' . With respect to the effects of ϕ and pressure, however, models accounting for flame stretch and instabilities, through the inclusion of model terms depending on thermodynamic mixture properties and pressure, had a slight edge on simpler formulations.

Keywords: methanol, spark-ignition engine, thermodynamic, modeling, turbulent burning velocity, constant volume bomb

1. Introduction

The use of light alcohols as spark-ignition engine fuels can help to increase energy security and offers the prospect of carbon neutral transport. Compared to other alternatives, such as hydrogen or battery-electric vehicles, liquid alcohols entail less issues regarding fueling and distribution infrastructure and are easily stored in a vehicle. In addition, the properties of these fuels enable considerable improvements in engine performance and efficiency as several investigations on converted gasoline engines have demonstrated [1].

In addition to bio-ethanol, methanol is interesting since it is versatile from a production point-of-view. Biofuels can only constitute part of our energy supply because of the limited area of arable land [2, 3]. Methanol, on the other hand, can be produced from a wide variety of renewable (e.g. gasification of wood, agricultural by-products and municipal waste) and alternative fossil fuel-based feed stocks (e.g. coal and natural

*Corresponding author. Tel.: +32(0)92643306; Fax: +32(0)92643590
Email address: sebastian.verhelst@ugent.be (S. Verhelst^a)
Preprint submitted to Elsevier

March 31, 2014

gas). A sustainable closed-carbon cycle where methanol is synthesized from renewable hydrogen and atmospheric CO₂ has been proposed [4].

To characterize the combustion behavior of methanol-air mixtures in practical applications, data for the laminar burning velocity are needed, together with a good understanding of the factors affecting turbulent burning velocities. The laminar burning velocity of methanol-air mixtures has been studied by the current authors in previous work [5, 6, 7, 8]. Turbulent burning velocity data for methanol-air mixtures are scarce, and difficult to compare due to reasons associated with the definition of the turbulent burning velocity as well as its dependency on experimental techniques and rigs [9].

This paper presents experimental values of the turbulent burning velocity of methanol-air mixtures measured during spherical explosions in a fan-stirred bomb. Measurements were made at rms turbulent burning velocities u' between 2 and 6 m/s, equivalence ratios between 0.8 and 1.4, pressures up to 0.5 MPa and at an initial temperature of 358 K. Next to obtaining better understanding of the different parameters affecting the burning velocity, an additional objective of this study was to assess to what degree the different models proposed in the literature can reproduce the trends observed over the full range of conditions investigated here. Therefore, comparisons have been made with data derived using several widely used turbulent burning velocity correlations.

2. Experimental methods

2.1. The Leeds Mk II combustion vessel

The turbulent burning velocity was measured using the spherically expanding flame technique. The experiments were performed in the Mk II high pressure fan-stirred combustion vessel at Leeds University. The details of the experimental apparatus have been extensively described in [10]. The spherical, stainless steel vessel has a 380 mm inner diameter and is capable of withstanding temperatures and pressures generated from explosions with initial pressures up to 1.5 MPa and initial temperatures up to 600 K [11]. The vessel is equipped with three pairs of orthogonal windows of diameter 150 mm. An electric heater at the wall provided up to 2 kW for preheating the vessel and mixture up to 358 K. Gas temperatures were obtained from a sheathed type-K thermocouple. Pressures were measured during the explosion with a Kistler type 701A pressure transducer. A central spark plug was used with ignition energies of about 23 mJ, supplied from a 12V transistorized automotive ignition coil. The spark gap was set to 1.2 mm for all present experiments.

Turbulence was generated in the vessel by four identical eight bladed fans in a regular tetrahedron configuration. These were also used to mix the reactants. The fans were directly coupled to electric motors with separate speed controllers. Each fan was separately adjustable between 200 and 10,000 rpm. The speed of individual fans was maintained within 5% of each other and adjusted to attain the required turbulence intensity. The rms turbulent velocity and integral length scale have been determined using Laser-Doppler Velocimetry (LDV) [9]. In the central, optically accessible region of the vessel, a reasonably uniform isotropic turbulence was found with u' given by Equation 1.

$$u'(\text{m/s}) = 0.00119f_s(\text{rpm}) \quad (1)$$

Where f_s is the fan speed in rpm. The estimated maximum deviation of u' from this equation is 10%. From a two-point correlation using a second LDV system the integral
80 length scale Λ was found to be 0.02 ± 0.001 m and was independent of all operating variables from 1000 to 10,000 rpm.

2.2. Schlieren flame photography

Following central spark ignition, the growth rate of spherically expanding flames was studied by high speed schlieren cine photography. This is a well established
85 method for flame imaging in combustion studies at Leeds University [12, 13]. A high speed Phantom digital camera with 256 megabytes integral image memory was used to capture flame propagation. The camera speed was between 5000 and 10,000 frames/s with 384 x 384 pixels, the resolution was 0.4065 mm/pixel. At small flame radii the measured flame speed is very sensitive to determination of the flame radius from the
90 digital images [14]. However, at these radii, the flame speed is affected by spark effects [10]. It was therefore decided to sacrifice spatial resolution at small radii in favor of higher frame rate and visibility of the entire vessel window area. In order to determine the turbulent burning velocity, image processing techniques were employed to automatically and robustly detect and reconstruct the flame front based on the maximum
95 grayness gradient in the schlieren images.

Due to the turbulent flame brush thickness, a problem particular to turbulent burning velocity measurements is the choice of the flame front surface to evaluate the burning velocity. This choice can affect the burning velocity by a factor up to 4 [15, 16]. This is shown diagrammatically in Figure 1. For a general spherical radius R_j , between
100 the flame root radius R_r and the flame tip radius R_t , there will be a certain mass of unburned gas m_{ui} and burned gas m_{bi} within that sphere, but outside the sphere of radius R_r . Similarly, outside a sphere of that radius, but within a radius of r_t , there will be a mass of unburned gas m_{uo} and burned gas m_{bo} .

In order to quantify the influence of the selected flame front surface on the burning
105 velocities obtained in the present rig, Bradley et al. performed simultaneous high speed photography of images from schlieren and laser sheet Mie scattering during spherical explosions [17]. This work yielded radial distributions of the progress variable \bar{c} , extending from a value of $\bar{c} = 0$ at R_r , to $\bar{c} = 1.0$ at R_r . An important result from their study is that for a certain radius r_v , at which the total volume of unburned gas inside
110 the sphere is equal to the total volume of burned gas outside it, the associated turbulent burning velocity, u_{tv} is given by the following simple expression:

$$u_{tv} = \frac{\rho_b}{\rho_u} \frac{dr_v}{dt} \quad (2)$$

In the present study, this basic expression was used to obtain u_t from the schlieren images. It was assumed that the radius R_{sch} , where the projected surface area of unburned gas inside it was equal to the projected surface area of burned gas outside it, was in
115 fact r_v . The work of Bradley et al. also yielded an empirical expression to relate this burning velocity to the turbulent velocity associated with the production of burned gas u_{tr} . This expression has been used throughout the rest of this work.

$$u_{tr} = 0.9 \frac{\rho_b}{\rho_u} \frac{dR_{sch}}{dt} \quad (3)$$

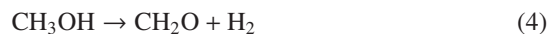
2.3. Mixture preparation

Before an explosion, the vessel was first flushed with dry air to remove most of the residuals from a previous experiment, after which it was evacuated down to 0.03 bar, filled with dry air to atmospheric pressure, and evacuated again to less than 0.03 bar. The liquid methanol volume to be injected into the bomb was found from the required molar mixture composition, the liquid methanol density and the known volume of the bomb. Liquid methanol was injected with a calibrated gas tight syringe, through a needle valve. Four syringes were employed, in this study, with volumes of 5, 10, 25 and 50 cm³, depending upon the volume of fuel required. Injection was carried out under vacuum at 0.03 bar and a temperature of 10-20 K higher than the ignition temperature, which aided methanol vaporization.

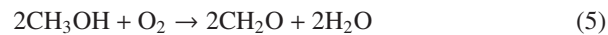
After injection the partial pressure and temperature of methanol vapor was measured in order to compare it with the theoretically required value resulting from the assumption of ideal gases. Next, the vessel was filled with dry air to the required initial pressure. Only conditions with the vapor pressure of methanol below the saturation pressure were studied here.

The mixture temperature was controlled by a CAL320PID controller in combination with a 2 kW electrical heater. As the heater coil is mounted inside the vessel, in contact with the mixture, it proved important to switch the heater off at least two minutes before injection and to leave it off till ignition. Failing to do so resulted in dissociation and partial oxidation of the methanol fuel, leading to low experimental repeatability. The chemical reactions at play are believed to be the following:

- In the absence of air (partial vacuum) the methanol can dissociate to formaldehyde and hydrogen. This reaction is associated with a large increase in partial pressure and can lead to burning velocities two to threefold the expected value, an effect of the high burning velocities of H₂ [18].



- When enough air is present (during filling with dry air) a partial oxidation of the methanol-air mixture can occur. This would lead to a mild increase in partial pressure (molar ratio of 4/3 between products and reactants) and a reduction in burning velocity due to the non-reactive water vapor.



When the heater is left on, the temperature in the vicinity of the heater coil will be a lot higher than the average mixture temperature so that these reactions can indeed be triggered.

3. Repeatability

At least three explosions were performed at each condition to obtain a measure for the repeatability of the experiments and to capture the stochastic variation associated with turbulent tests. In between experiments, the recorded pressure traces were used to quickly assess the repeatability by ensuring there was less than 5% variation in the time to reach a pressure rise of 50%. After processing the images, the standard deviation on the turbulent burning velocity was calculated as a function of flame radius for each condition.

The principal uncertainty was in making up the mixture. Therefore, factors affecting mixture stoichiometry were accurately controlled.

- The consistency of pressure and temperature just prior to ignition was of importance. The tolerance for these parameters was set at ± 0.02 bar and ± 3 K respectively.
- Residuals were considered as another source affecting mixture composition, but were kept at a minimum through adequate flushing of the vessel after each experiment.
- The hygroscopic nature of methanol could affect the fuel purity. Therefore, methanol was stored in small 50 ml flasks, minimizing the contact with ambient air. The water content of methanol stored in such a way during the entire course of this work was checked and proved to be below 1 % by mass.
- Another factor was the uncertainty of the full scale deflection of the syringe used to inject methanol. The manufacturer tolerance was given as 0.5 % at full scale. This would correspond to an average uncertainty on the equivalence ratio of below 1.5 % [13].
- A final influence was the vessel sealing. Although the seals were replaced during the initial stages of this work, still some degree of leakage was present. This is particularly important for the measurements at elevated pressures. At these conditions part of the methanol-air mixture leaks during the addition of dry air, which affects stoichiometry. The leakage rate was estimated by measuring the rate of pressure decrease after the vessel had been pressurized to 5 bar and was in the order of 0.01 bar per minute. Pressurizing the vessel took around 3 minutes. The worst case effect on ϕ , assuming that all leakage consists of fuel vapor and the leakage is at its maximal rate throughout the pressurization, is below 5%.

Although the mixture stoichiometry was controlled by injecting a known amount of methanol, the correct composition of the mixture was cross-checked by comparing measured partial pressures of methanol vapor to the theoretical value assuming ideal gas behavior.

It appeared that the measured partial pressure of methanol vapor was consistently 5-10 % lower than the theoretical value, which means the actual mixture equivalence ratio was lower than the desired value by the same percentage. This was found to be due to fuel absorption on carbon deposits in the vessel's seal cavities. Most models

predict the turbulent burning velocity based on the laminar burning velocity at the same conditions. Since the laminar burning velocity values used in this work were measured using the same setup [8] and consequently suffer from a similar divergence in ϕ , the divergence should have no effect on the qualitative trends predicted by the models. In
195 the following, the results are therefore presented as function of the desired value of ϕ and not as function of the correct ϕ based on partial pressure, as was done in [8].

4. Measurement conditions

Turbulent methanol-air flames were measured at two pressures (1 and 5 bar), five
200 desired equivalence ratios ($\phi=0.8, 1.0, 1.2, 1.4, 1.6$) and three rms turbulent velocities ($u' = 2, 4, 6$ m/s). All measurements were done at 358 K. Table 1 lists the measurement conditions. Table 2 summarizes the mixture Lewis number Le , measured laminar burning velocity u_l and Markstein length L_b measured at the same conditions. These values are discussed in more detail in [8].

205 For some conditions, marked by * in Table 1, less than 3 repetitions were performed, so the results should be handled with care. For lean mixtures, flame quenching can occur at elevated values of u' . This is marked by a 'q' in the table.

5. Observations of spherically propagating turbulent methanol flames

Shown in Figure 2 are schlieren images of stoichiometric methanol-air flames ($\phi=1.0$)
210 as a function of time after ignition, for different initial pressures and u' . Figure 3 shows the same for a rich mixture ($\phi=1.4$). For each measurement condition, multiple experiments were conducted and one representative experiment is shown in the figures. Both figures show how the wrinkling of turbulent flames increases with u' , resulting in a faster flame propagation.

215 The flames at 1 bar and elevated turbulence ($u'=6$ m/s) are heavily distorted and convected away from the spark gap. This decreases the accuracy of representing flames as expanding spherically from the point of ignition. Explosions at elevated pressure ($p=5$ bar) show that not only the centroid of the flame is closer to the spark gap, but flames are more spherical in appearance. Mansour suggests that the amount of flame
220 distortion is related to the Markstein number. Flames with higher positive Ma at high u' are locally slower and consequently more distorted and partially quenched, as illustrated in Figure 2 ($p=1$ bar, $u'=6$ m/s).

The same Markstein number effect might explain why the rich methanol flames seem to cope better with turbulence. For comparable conditions, the rich turbulent
225 flames ($\phi=1.4$; $L_b=0.55$ mm at 1 bar, -0.26 mm at 5 bar) propagate faster and less distorted than the stoichiometric flames ($\phi=1.0$; $L_b=0.85$ mm at 1 bar, 0.05 mm at 5 bar) although their laminar burning velocity is lower. A faster turbulent flame speed in spite of reduced u_l also applies when comparing the results at elevated pressure to those at 1 bar. The lower Markstein number at 5 bar leads to less reduction in local flame speed
230 due to stretch. Additionally, the inherent laminar instability of rich flames at elevated pressures can produce a more finely wrinkled flame, further increasing the turbulent flame speed.

6. Turbulent burning velocities versus radius

Figure 4 shows the turbulent mass burning velocity u_{tr} (according to Eq. 3) plotted as a function of mean schlieren radius r_{sch} . Figure 4 illustrates the influence of u' at different equivalence ratios. A first thing to notice is that after an initial period of spark affected flame propagation ($r_{sch} < 10$ mm) u_{tr} rises as the flame radius grows. This well known phenomenon arises because, in the early stage of flame propagation, the flame can only be wrinkled by length scales less than the size of the flame kernel [16]. As a consequence, the rms turbulent burning velocity effective in wrinkling the flame front, u'_k , is less than the value measured in the bomb in the absence of any flame (u') [16].

Two obvious trends can be identified from Figure 4. The first is that u_{tr} obviously increases with u' through more intense flame front wrinkling. As the turbulence intensity rises, so does the stochastic variation on u_{tr} . Mansour attributes this to the increasing importance of merging and quenching effects, and the associated distortion in spherical flame front shape, at higher values of u' [13]. A second trend is that the turbulent burning velocity grows with pressure, especially for rich mixtures, despite a decreased laminar burning velocity. As mentioned before, this can be attributed to lower Markstein numbers and the effects of preferential diffusion and flame instabilities.

7. Qualitative trends

To distinguish qualitative trends of turbulent burning velocity as a function of u' , ϕ and p , and to quantitatively compare the experimental values of u_{tr} to model predictions, the flame velocity at a fixed mean flame radius of 30 mm was selected to provide a single representative value of u_{tr} . This radius is large enough to discount any spark effects and is small enough to ensure that most flames grew to this radius before parts of the flame edge extended beyond the window due to bulk flame convection effects [9].

Figure 5 plots the turbulent burning velocity at 30 mm ($u_{tr,30mm}$) versus rms velocity u' for methanol-air flames at 1 and 5 bar. It is clear that the turbulent burning velocities can be well approximated by a linear correlation with u' , with some slight downward bending.

In Figure 6 the same results are replotted as $u_{tr,30mm}$ normalized by u_l versus the ratio of u' to u_l . Linear fits are also shown. Whereas Verhelst reported an almost perfect fit very close to $u_{tr,30mm} = u' + u_l$ for hydrogen-air flames, this is not the case for the current results [19]. This can be partly due to the experimental uncertainty on $u_{tr,30mm}$ and u_l , but also indicates that for alcohol-air flames at these conditions, factors other than u_l and u' are important to the turbulent flame development.

To further illustrate this, Figure 7 shows the turbulent burning velocity ratio $u_{tr,30mm}/u_l$ as a function of equivalence ratio ϕ . The ratio $u_{tr,30mm}/u_l$ can be seen to remain fairly constant with equivalence ratio. At 5 bar, there is a slight rise for the leanest and richest mixtures. The figures also confirm that $u_{tr,30mm}/u_l$ rises as the pressure increases. These two observations are in line with the differential diffusion theory [20]. As the molecular weight of methanol is the same as that of O_2 ($M=32$ g/mol), its molecular

275 diffusivity will be comparable. This means the Lewis number will be largely independent of ϕ and the effects of preferential diffusion are limited. Note that the present results for methanol at 5 bar, $u'=2$ m/s correspond well to the values of Lawes et al [21], especially when keeping in mind that the real ϕ is 5-10% lower than the desired ϕ displayed here.

280 8. Model comparison

8.1. Model implementation and calibration

The turbulent methanol-air measurements described above are used to evaluate the predictive capabilities of several turbulent burning velocity models. The unburned gas mixture properties used in the model equations (e.g. ν , ρ_u) were calculated using a thermodynamic database [22]. The laminar burning velocities and Lewis numbers of the different mixtures are summarized in Table 2. An assumption in various models, $u' \gg u_l$, is generally satisfied here.

Numerous models and correlations exist to predict the turbulent burning velocity and unfortunately no single model has emerged as the most accurate or most widely applicable. For this work, a selection is made of models that have been widely demonstrated and used in simulation of SI engines or other combustion applications. Lipatnikov and Chomiak [23] tested a variety of models and concluded that only a few expressions can predict all the experimental trends they observed in the body of literature: those of Zimont/Lipatnikov [24, 23], Peters [25] and the Coherent Flame Model (CFM) [26]. Fractal-based models [27, 28] were reported to reproduce many trends.

285 These and other models used in this work are described in the Appendix and the corresponding original references. The model formulations are slightly adapted here to correspond to the way they would be used in a combustion simulation code. This involved adding a calibration factor C_2 and a term u_n to ensure the stretched laminar burning velocity u_n appears when $u' \rightarrow 0$. The expressions are used here to directly calculate the mass consumption velocity u_{tr} .

- Damköhler:

$$u_t = C_2 u' + u_n \quad (6)$$

- Gülder:

$$u_t = 0.6 C_2 u'^{0.5} u_n^{0.5} Re_t^{0.25} + u_n \quad (7)$$

- Bradley $KaLe$:

$$u_t = 0.88 C_2 u' (KaLe)^{-0.3} + u_n \quad (8)$$

- 305 • Bradley $KaMa$:

$$u_t = 0.54 C_2 \alpha (Ka)^\beta + u_n \quad (9)$$

- Fractals:

$$u_t = u_n (Re_t)^{0.75(D_3-2)} \quad (10)$$

$$D_3 = \frac{2.35 C_2 u'}{u' + u_n} + \frac{2.0 u_n}{u' + u_n} \quad (11)$$

- Peters:

$$u_t = 0.195C_2u'Da \left[\left(1 + \frac{30.52}{Da} \right)^{0.5} - 1 \right] + u_n \quad (12)$$

- Zimont:

$$u_t = C_2u'Da^{1/4} + u_n \quad (13)$$

- Dinkelacker:

$$u_t = u_n + \frac{0.46C_2 \cdot u_n}{Le} Re_i^{0.25} \left(\frac{u'}{u_n} \right)^{0.3} \left(\frac{p}{p_0} \right)^{0.2} \quad (14)$$

310

- Kolla:

$$\frac{u_t}{u_l} = \left\{ \frac{18C_2}{(2C_m - 1)\beta'} \left[[2K_c^* - \tau C_4] \left(\frac{u'\Lambda}{u_l\delta_l} \right) + \frac{2C_3}{3} \left(\frac{u'}{u_l} \right)^2 \right] \right\}^{1/2} \quad (15)$$

- Coherent Flame Model: this model is used in its original form with the fitted function for Γ represented by Equations A.21 - A.26. For this choice of Γ the model is calibrated by varying the constant C in Equation A.19.

As mentioned above, only part of the turbulent spectrum is effective in wrinkling the flame. To account for this flame development, the effective rms turbulent burning velocity u'_k is used instead of u' in the model formulations. Bradley et al. developed an expression for u'_k based on a large experimental dataset and the integration of the power spectral densities of eddies inside the bomb between the Kolmogorov scale and a limiting scale in the bomb [16]. The value for u'_k is calculated based on this work. For the Coherent Flame Model, the temporal development of flame wrinkling is implemented by solving the balance equation for the flame surface density Σ (Eq. A.18). The calibration constants are chosen in such a way that the model prediction exactly matches the measured burning velocity $u_{tr,30mm}$ at 1 bar, $\phi=1.0$ and $u'=2$ m/s.

8.2. Model comparison

In what follows, the turbulent burning velocity models are tested for varying rms turbulent velocity and varying equivalence ratio. The results are displayed in terms of $u_{tr,30mm}$ vs. u' and $u_{tr,30mm}/u_l$ vs ϕ plots. Experimental results are marked by the closed symbols, while the open symbols represent model results. A selection of the most promising models is made at the end of this section. The models' performance is demonstrated using some selected plots. Further modeling results can be found in Electronic Supplementary Material.

8.2.1. Damköhler

As could be expected from the model equations, Figure 8 illustrates that the predicted trend for u_t versus u' is linear, leading to an overprediction of u_t at high values of u' . The results for u_t/u_l show good correspondence for stoichiometric to rich mixtures (Figure 9). For lean mixtures, the simulated ratio u_t/u_l is too high, probably because the calculated u_t is primarily defined by u' at those conditions (see Eq. 6). The results

suggest that the effects of pressure on u_t/u_l are not well represented by the Damköhler model. The results for the Peters model are very similar (not shown here), which could be expected since both models are the same in the limit for large Damköhler numbers [12].

8.2.2. Gülder

The model equations of Gülder correctly reproduce the bending of the u_t vs. u' curve (see Figure 10). The evolution of u_t/u_l with ϕ is well predicted by the Gülder model (Figure 11). The underprediction of the effect of pressure on u_t/u_l is less pronounced than for the Damköhler model.

8.2.3. Bradley

The $KaLe$ correlation of Bradley et al. also reproduces the bending of the u_t vs. u' curve (not shown here). The u_t/u_l vs. ϕ evolution is well predicted, except maybe for the richest mixtures, where there is a slight underestimation (see Figure 13). The results illustrate a striking underestimation of the effect of pressure on u_t/u_l (see Figure 13). This is possibly due to the insensitivity of the Lewis number to pressure. Note that the effect of this underestimation on the predicted u_t will be lower at elevated, engine-like pressures, because u_l varies only slightly with pressure at these conditions.

To introduce the effect of pressure on flame dynamics, Bradley et al. [16] recently proposed a correlation for u_t/u' as a function of Ka and Ma_{sr} based on spherical explosions and twin kernel implosions in a fan-stirred bomb of ethanol-air mixtures for a wide range of ϕ , p and u' . The correlation reflects that, at constant Ka , there is an increased rate of burning in laminar flamelets, independent of that due to wrinkling, as Ma_{sr} is decreased in the predominantly positively stretched flames. At higher Ka , flame front merging and extinction lead to a decrease in u_t/u' .

8.2.4. Fractals

The fractal model underestimates the slope of the u_t vs. u' curve, especially at higher pressures (Figure 14). This model does not reproduce the rise in u_t/u_l for rich mixtures, as becomes clear from Figure 15. Also, it gives the worst underestimation of the effect of pressure on u_t/u_l among the models considered here. It was attempted to include the effect of stretch on the local burning velocity u_n by applying the stretch submodels of both Teraji et al. [29] and Chung & Law [30, 31]. The model of Teraji et al. did not enable any significant improvements. That of Chung & Law is only valid for small values of Ka and produced negative values of u_t for the highly turbulent flames considered here.

8.2.5. Zimont

The trends predicted by the model of Zimont agree well with those observed experimentally (see Figures 18 and 19). For the richest mixtures, there is a slight underprediction of u_t/u_l , but the representation of the pressure effect on u_t/u_l is one of the best among the models considered here. The model of Kerstein [32] was also evaluated and as suggested by Lipatnikov and Chomiak, its performance is very close to that of the Zimont model [23] (not shown here).

8.2.6. *Dinkelacker*

380 As can be seen in Figures 20 and 21 the predictive performance of the Dinkelacker model in terms of equivalence ratio and pressure is very good. The inclusion of a pressure dependent term in Equation 14 leads to the best representation of the pressure effect among the models evaluated here.

8.2.7. *Kolla*

385 The model of Kolla et al. performs rather poorly (see Figures 22 and 23). The bending of the u_t vs. u' curve is reproduced but the slope of the curve is underestimated. Also, u_t/u_l is predicted to be insensitive to equivalence ratio, which is in disagreement with the experimental results.

8.2.8. *Coherent Flame Model*

390 Figures 24 and 25 display the Coherent Flame model performance for Γ according to Eqs. A.21 - A.26. The slope of the u_t vs u' curve is too high. This is an indication that the model equations do not correctly reproduce the flame development as encountered in the spherical flames. The use of the effective rms turbulent velocity u'_k in these equations improves the correspondence to experiments (not shown here).

395 The effect of pressure on u_t is mainly implemented through the dependence of Γ on laminar flame thickness δ_l . The stretch efficiency function was derived for engine-like, high pressure conditions. At the moderate pressure conditions considered here, δ_l varies significantly with pressure, which might explain the exaggerated response of u_t to pressure.

400 The effect of equivalence ratio on u_t/u_l is well reproduced for stoichiometric and rich mixtures, but heavily overestimated u_t/u_l at lean conditions. Possibly this is due to the fact that Γ was primarily fitted to results obtained for stoichiometric flames.

8.3. *Conclusions*

405 In the current work, the turbulent combustion behavior of methanol was evaluated based on turbulent burning velocity measurements obtained in a fan-stirred bomb. The results indicate that the effect of rms turbulent velocity u' on u_t is well represented by most models. It is slightly underestimated by the Fractals and Kolla model, and considerably overestimated by the CFM model. The models of Dinkelacker, Zimont, Bradley *KaLe* and Gülder perform best as they reproduce the effects of varying
410 ϕ through the inclusion of thermodiffusive mixture properties. For most models there was an underprediction of the effect of pressure on u_t . The thermodiffusive properties in these models do not depend on pressure and consequently cannot reflect the effects of reduced flame stretch effects and increased flame wrinkling at higher pressures. The Dinkelacker model performed best in this respect through the inclusion of a pressure
415 dependent term in the model formulation. The Coherent Flame Model arguably performed the worst among the models considered here. Possibly this is because the model was developed with the explicit goal of engine simulations in mind and its direct dependence on flame thickness is not valid at the moderate pressures during bomb experiments. Future model developments should focus on reproducing the effects of
420 pressure on the flame phenomenology. One approach could be to include measured Markstein numbers, which depend on pressure, in the model expressions.

Acknowledgements

J. Vancoillie gratefully acknowledges a Ph. D. fellowship (FWO09/ASP/030) and a travel grant for a long stay abroad (V407312N) of the Research Foundation - Flanders.

References

References

- [1] J. Vancoillie, J. Demuynck, L. Sileghem, M. Van De Ginste, S. Verhelst, L. Brabant, L. Van Hoorebeke, The potential of methanol as a fuel for flex-fuel and dedicated spark-ignition engines, *Applied Energy* 102 (2013) 140–149.
- [2] M. Specht, A. Bandi, Renewable carbon-based transportation fuels, Vol. 3C of Renewable Energy, Springer Berlin Heidelberg, Berlin, 2006.
- [3] R. Pearson, J. Turner, A. Peck, Gasoline-ethanol-methanol tri-fuel vehicle development and its role in expediting sustainable organic fuels for transport, in: IMechE Low Carbon Vehicles Conference, London, UK, 2009, pp. 1–21.
- [4] G. Olah, A. Goeppert, G. Prakash, Beyond Oil and Gas: the Methanol Economy., Wiley-VCH Verlag GmbH & Co.KGaA, Weinheim, Germany, 2006.
- [5] J. Vancoillie, M. Christensen, E. J. K. Nilsson, S. Verhelst, A. A. Konnov, Temperature dependence of the laminar burning velocity of methanol flames, *Energy & Fuels* 26 (3) (2012) 1557–1564.
- [6] J. Vancoillie, M. Christensen, E. J. K. Nilsson, S. Verhelst, A. A. Konnov, The effects of dilution with nitrogen and steam on the laminar burning velocity of methanol at room and elevated temperatures, *Fuel* 105 (2013) 732–738.
- [7] J. Vancoillie, S. Verhelst, J. Demuynck, Laminar burning velocity correlations for methanol-air and ethanol-air mixtures valid at SI engine conditions, SAE International, SAE paper no. 2011-01-0846 (2011).
- [8] J. Vancoillie, G. Sharpe, M. Lawes, S. Verhelst, Laminar burning velocities and markstein lengths of methanol-air mixtures at pressures up to 1.0 mpa, submitted to *Fuel* (2014).
- [9] M. Lawes, M. P. Ormsby, C. G. W. Sheppard, R. Woolley, The turbulent burning velocity of iso-octane/air mixtures, *Combustion and Flame* 159 (5) (2012) 1949–1959.
- [10] D. Bradley, M. Lawes, M. S. Mansour, Explosion bomb measurements of ethanol-air laminar gaseous flame characteristics at pressures up to 1.4 MPa, *Combustion and Flame* 156 (7) (2009) 1462–1470.
- [11] D. Bradley, R. A. Hicks, M. Lawes, C. G. W. Sheppard, R. Woolley, The measurement of laminar burning velocity and markstein numbers for iso-octane-air and iso-octane-n-heptane-air mixtures at elevated temperatures and pressures in an explosion bomb, *Combustion and Flame* 115 (1-2) (1998) 126–144.

- 460 [12] S. Verhelst, R. Sierens, A quasi-dimensional model for the power cycle of a hydrogen-fuelled ICE, *International Journal of Hydrogen Energy* 32 (15) (2007) 3545–3554.
- [13] M. S. Mansour, Fundamental study of premixed combustion rates at elevated pressure and temperature, Ph.D. thesis, University of Leeds (2010).
- 465 [14] S. Y. Liao, D. M. Jiang, Z. H. Huang, W. D. Shen, C. Yuan, Q. Cheng, Laminar burning velocities for mixtures of methanol and air at elevated temperatures, *Energy Conversion and Management* 48 (3) (2007) 857–863.
- [15] J. F. Driscoll, Turbulent premixed combustion: Flamelet structure and its effect on turbulent burning velocities, *Progress in Energy and Combustion Science* 34 (1) (2008) 91–134.
- 470 [16] D. Bradley, M. Lawes, M. S. Mansour, Correlation of turbulent burning velocities of ethanol-air, measured in a fan-stirred bomb up to 1.2 MPa, *Combustion and Flame* 158 (1) (2010) 123–138.
- [17] D. Bradley, M. Z. Haq, R. A. Hicks, T. Kitagawa, M. Lawes, C. G. W. Sheppard, R. Woolley, Turbulent burning velocity, burned gas distribution, and associated flame surface definition, *Combustion and Flame* 133 (4) (2003) 415–430.
- 475 [18] S. Verhelst, R. Woolley, M. Lawes, R. Sierens, Laminar and unstable burning velocities and markstein lengths of hydrogen-air mixtures at engine-like conditions, *Proceedings of the Combustion Institute* 30 (2005) 209–216.
- [19] S. Verhelst, A study of the combustion in hydrogen-fuelled internal combustion engines., Ph.D. thesis, Ghent University, doi: dx.doi.org/1854/3378 (2005).
- 480 [20] A. N. Lipatnikov, J. Chomiak, Molecular transport effects on turbulent flame propagation and structure, *Progress in Energy and Combustion Science* 31 (1) (2005) 1–73.
- [21] M. Lawes, M. P. Ormsby, C. G. W. Sheppard, R. Woolley, Variation of turbulent burning rate of methane, methanol, and iso-octane air mixtures with equivalence ratio at elevated pressure, *Combustion Science and Technology* 177 (7) (2005) 1273 – 1289.
- 485 [22] C. Morley. GASEQ: a chemical equilibrium program for Windows [online] (2005) [cited July 10th 2012].
- 490 [23] A. N. Lipatnikov, J. Chomiak, Turbulent flame speed and thickness: phenomenology, evaluation, and application in multi-dimensional simulations, *Progress in Energy and Combustion Science* 28 (1) (2002) 1–74.
- [24] V. L. Zimont, Gas premixed combustion at high turbulence. turbulent flame closure combustion model, *Experimental Thermal and Fluid Science* 21 (1-3) (2000) 179–186.
- 495

- [25] N. Peters, *Turbulent Combustion*, Cambridge University Press, Cambridge, 2000.
- [26] S. Richard, S. Bougrine, G. Font, F.-A. Lafossas, F. L. Berr, On the reduction of a 3D CFD combustion model to build a physical 0D model for simulating heat release, knock and pollutants in SI engines, *Oil and Gas Science and Technology - Rev. IFP* 64 (3) (2009) 223–242.
- 500 [27] Y.-W. Chin, R. D. Matthews, S. P. Nichols, T. M. Kiehne, Use of fractal geometry to model turbulent combustion in SI engines, *Combustion Science and Technology* 86 (1) (1992) 1 – 30.
- [28] C.-M. Wu, C. E. Roberts, R. D. Matthews, M. J. Hall, Effects of engine speed on combustion in si engines: Comparisons of predictions of a fractal burning model with experimental data, SAE International, SAE paper no. 932714 (1993).
- 505 [29] A. Teraji, A. Gurupatham, Development of flame propagation model considering Lewis number effect for fast idle condition, SAE International, SAE paper no. 2011-01-1892 (2011).
- [30] W. Dai, G. C. Davis, M. J. Hall, R. D. Matthews, Diluents and lean mixture combustion modeling for si engines with a quasi-dimensional model, SAE International, SAE paper no. 952382 (1995).
- 510 [31] C. D. Rakopoulos, C. N. Michos, E. G. Giakoumis, Thermodynamic analysis of si engine operation on variable composition biogas-hydrogen blends using a quasi-dimensional, multi-zone combustion model, SAE International, SAE paper no. 2009-01-0931 (2010).
- 515 [32] A. R. Kerstein, A linear-eddy model of turbulent scalar transport and mixing, *Combustion Science and Technology* 60 (4-6) (1988) 391–421.
- [33] O. L. Gülder, Turbulent premixed flame propagation models for different combustion regimes, *Symposium (International) on Combustion* 23 (1) (1991) 743–750.
- 520 [34] R. G. Abdel-Gayed, D. Bradley, M. Lawes, Turbulent burning velocities: A general correlation in terms of straining rates, *Proceedings of the Royal Society of London. A. Mathematical and Physical Sciences* 414 (1847) (1987) 389–413.
- [35] F. Bozza, A. Gimelli, S. S. Merola, B. Vaglieco, Validation of a fractal combustion model through flame imaging, SAE International, SAE paper no. 2005-01-1120 (2005).
- 525 [36] F. Bozza, A. Gimelli, L. Strazzullo, E. Torella, C. Cascone, Steady-state and transient operation simulation of a downsized turbocharged SI engine, SAE International, SAE paper no. 2007-01-0381 (2007).
- [37] R. D. Matthews, M. J. Hall, W. Dai, G. C. Davis, Combustion modeling in SI engines with a peninsula-fractal combustion model, SAE International, SAE paper no. 960072 (1996).
- 530

- [38] S. P. R. Muppala, N. K. Aluri, F. Dinkelacker, A. Leipertz, Development of an algebraic reaction rate closure for the numerical calculation of turbulent premixed methane, ethylene, and propane/air flames for pressures up to 1.0 mpa, *Combustion and Flame* 140 (4) (2005) 257–266.
- [39] H. Kobayashi, Y. Kawabata, K. Maruta, Experimental study on general correlation of turbulent burning velocity at high pressure, *Symposium (International) on Combustion* 27 (1) (1998) 941–948.
- [40] H. Kolla, J. W. Rogerson, N. Swaminathan, Validation of a turbulent flame speed model across combustion regimes, *Combustion Science and Technology* 182 (3) (2010) 284 – 308.
- [41] A. Teraji, T. Tsuda, T. Noda, M. Kubo, T. Itoh, Development of a novel flame propagation model (UCFM: Universal coherent flamelet model) for SI engines and its application to knocking prediction, *SAE International*, SAE paper no. 2005-01-0199 (2005).
- [42] F. Charlette, C. Meneveau, D. Veynante, A power-law flame wrinkling model for les of premixed turbulent combustion. part i: Non-dynamic formulation and initial tests, *Combustion and Flame* 131 (1-2) (2002) 159–180.

Table 1: Measured conditions for turbulent methanol-air flames. Quenched flames are indicated by q . * denotes conditions that were measured less than 3 times

p	1 bar			5 bar		
T_u	358 K			358 K		
ϕ	u' (m/s)			u' (m/s)		
0.8	2*	4	6 q	2	-	-
1.0	2	4	6	2	4	6
1.2	2	4	6	2	4*	-
1.4	2	4	6	2	4	6
1.6	2*	-	-	-	-	-

Table 2: Laminar burning velocities and Lewis numbers for turbulent methanol-air flames

p	1 bar			5 bar		
T_u	358 K			358 K		
ϕ	u_l (m/s)	L_b (mm)	Le	u_l (m/s)	L_b (mm)	Le
0.8	0.319	+0.92	1.04	0.182	+0.41	1.04
1.0	0.496	+0.85	0.96	0.337	+0.05	0.96
1.2	0.588	+0.73	0.89	0.421	-0.13	0.89
1.4	0.591	+0.55	0.85	0.395	-0.26	0.85
1.6	0.503	+0.40	0.82	-	-	-

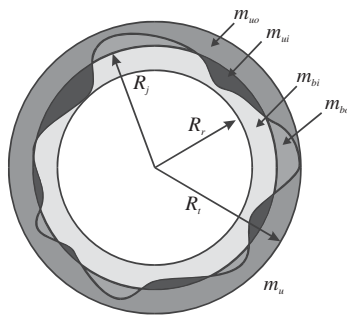


Figure 1: Masses of burned and unburned gas at a given instant during spherical explosive propagation. Mass of unburned gas inside sphere of radius R_j is m_{ui} , mass of burned gas outside it is m_{bo} . From [17]

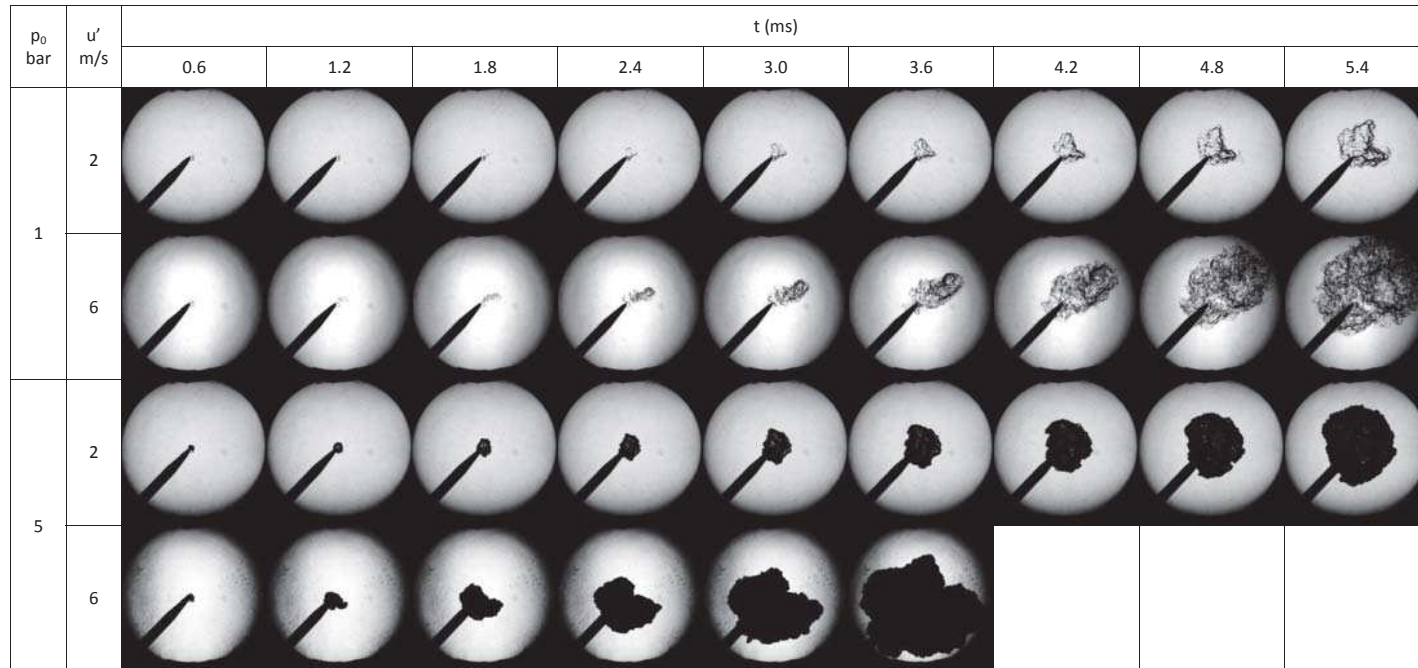


Figure 2: Turbulent flame propagation in a stoichiometric methanol-air mixture ($\phi = 1.0$) at an initial temperature of 358K and different initial pressures ($p = 1, 5$ bar) and rms turbulent velocities ($u' = 2, 6$ m/s).

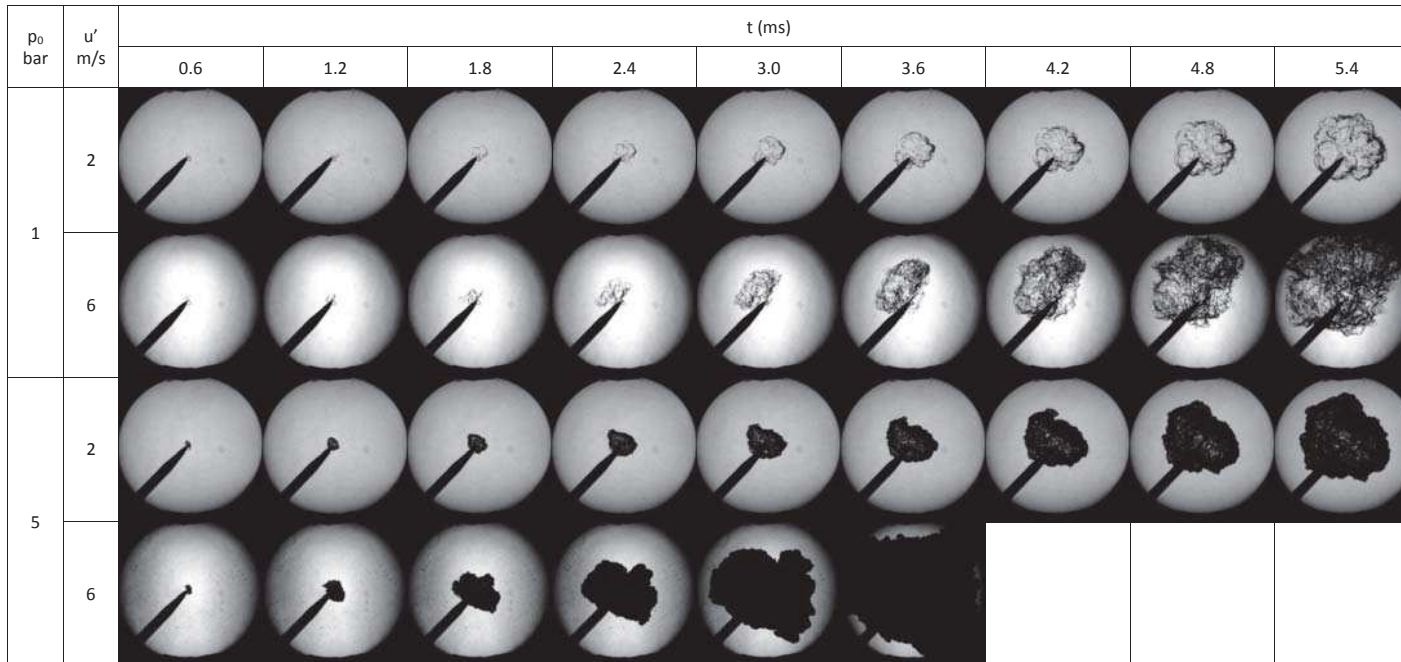


Figure 3: Turbulent flame propagation in a rich methanol-air mixture ($\phi = 1.4$) at an initial temperature of 358K and different initial pressures ($p = 1, 5$ bar) and rms turbulent velocities ($u' = 2, 6$ m/s).

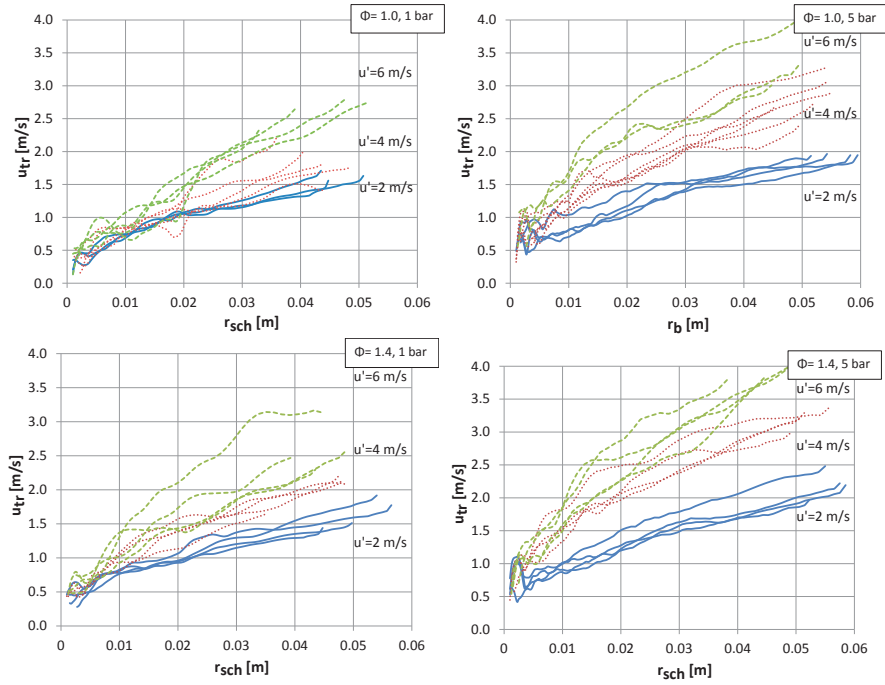


Figure 4: Burning velocity u_{tr} versus mean schlieren radius r_{sch} ($T_u=358 \text{ K}$). The turbulent burning velocity increases with u' through more intense flame front wrinkling

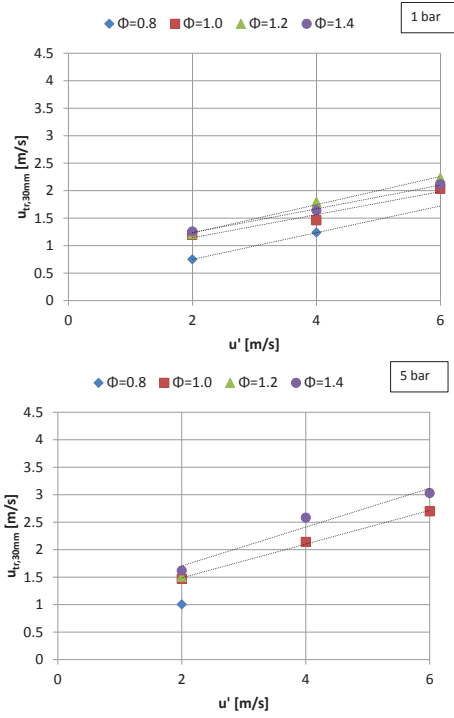


Figure 5: Burning velocity $u_{tr,30mm}$ versus u' ($T_u=358$ K)

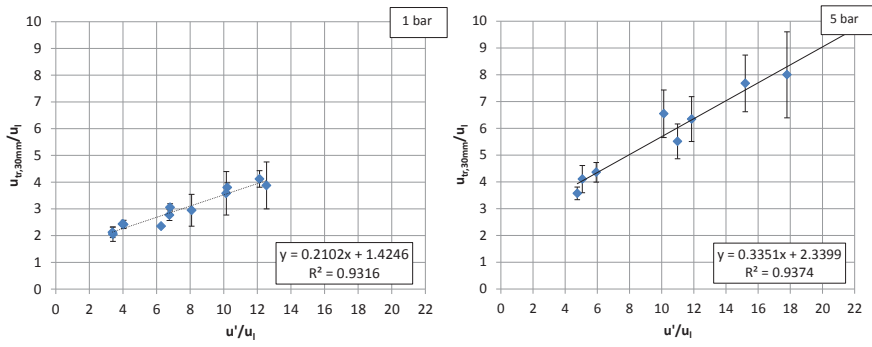


Figure 6: $u_{tr,30mm}/u_l$ versus u'/u_l ($T_u=358$ K)

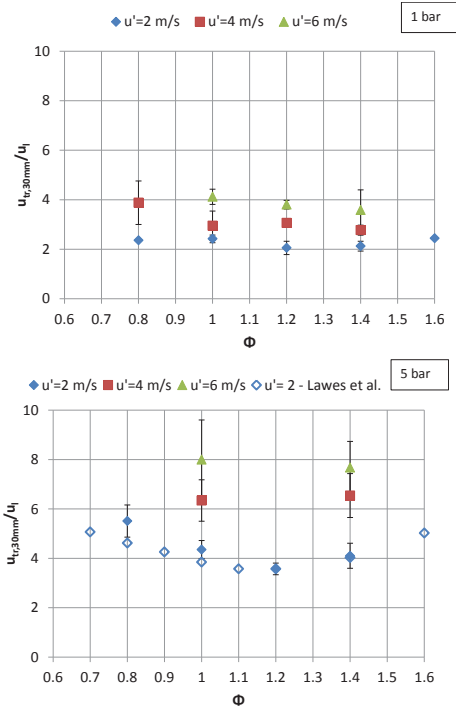


Figure 7: $u_{tr,30mm}/u_l$ versus ϕ ($T_u=358$ K)

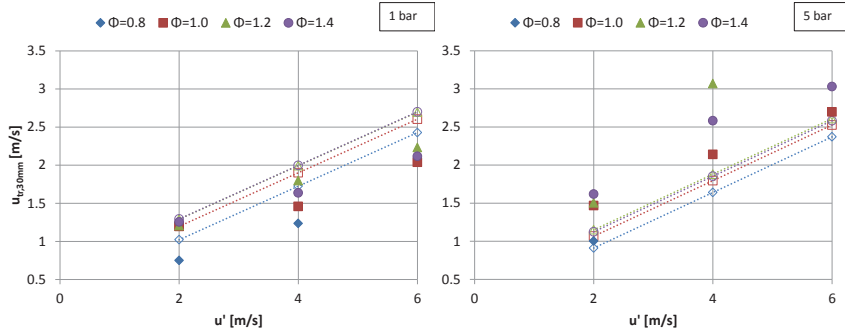


Figure 8: $u_{tr,30mm}$ vs. u' for the Damköhler model. Closed symbols - experiment, open symbols - model.

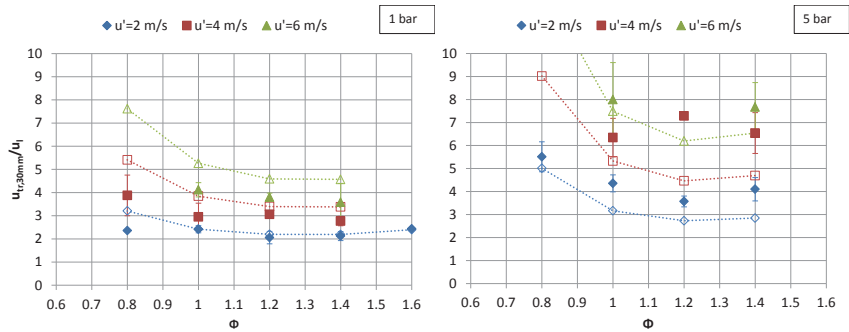


Figure 9: $u_{tr,30mm}/u_l$ vs. ϕ for the Damköhler model. Closed symbols - experiment, open symbols - model.

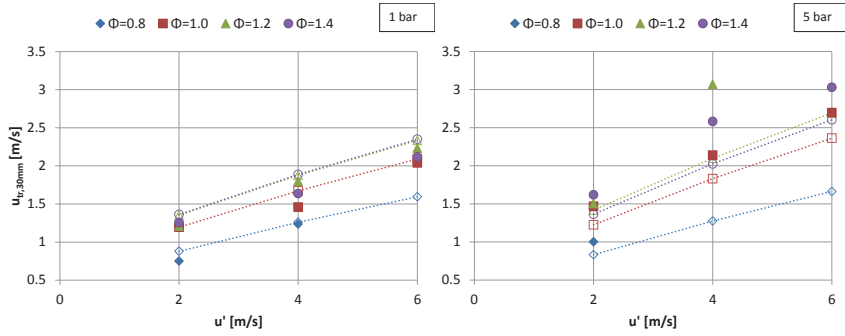


Figure 10: $u_{tr,30mm}$ vs. u' for the Gülder model. Closed symbols - experiment, open symbols - model.

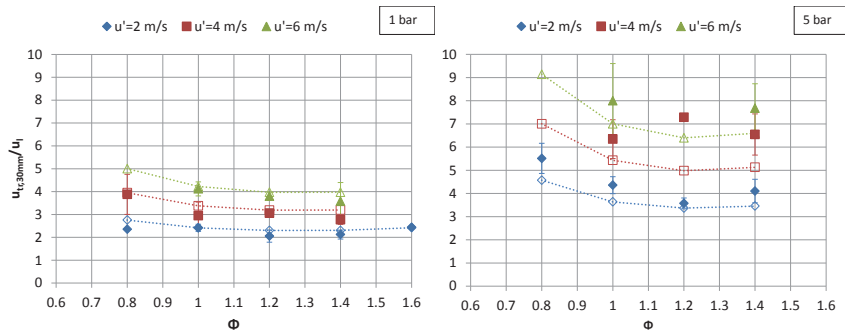


Figure 11: $u_{tr,30mm}/u_l$ vs. ϕ for the Gülder model. Closed symbols - experiment, open symbols - model.

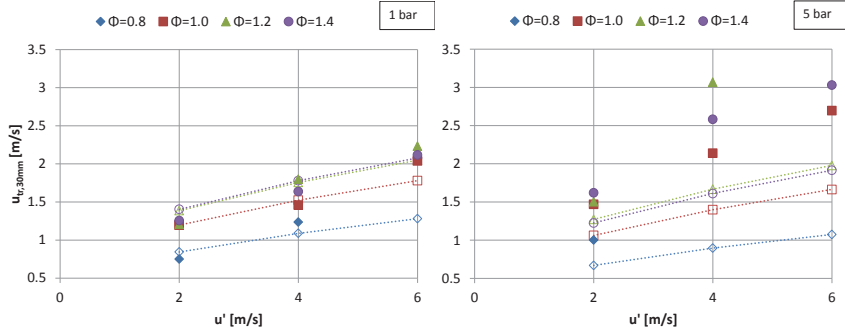


Figure 12: $u_{tr,30mm}$ vs. u' for the *KaLe* model of Bradley et al. Closed symbols - experiment, open symbols - model.

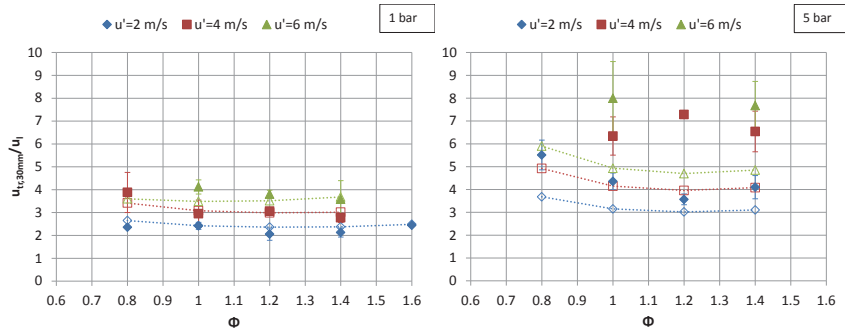


Figure 13: $u_{tr,30mm}/u_l$ vs. ϕ for the *KaLe* model of Bradley et al. Closed symbols - experiment, open symbols - model.

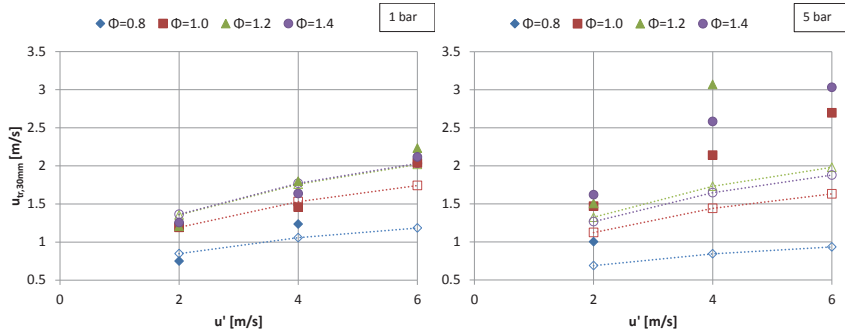


Figure 14: $u_{tr,30mm}$ vs. u' for the Fractals model. Closed symbols - experiment, open symbols - model.

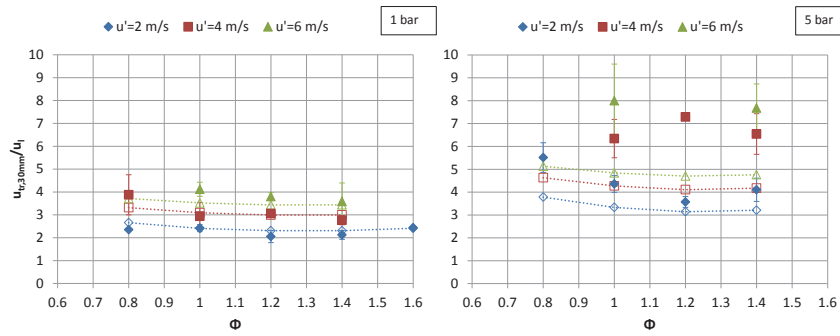


Figure 15: $u_{tr,30mm}/u_l$ vs. ϕ for the Fractals model. Closed symbols - experiment, open symbols - model.

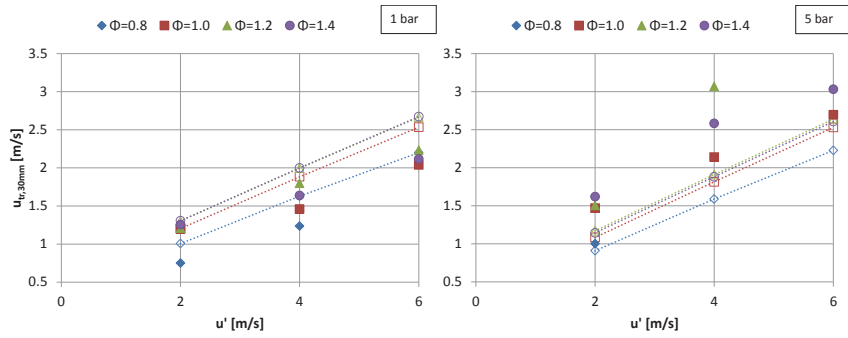


Figure 16: $u_{tr,30mm}$ vs. u' for the Peters model. Closed symbols - experiment, open symbols - model.

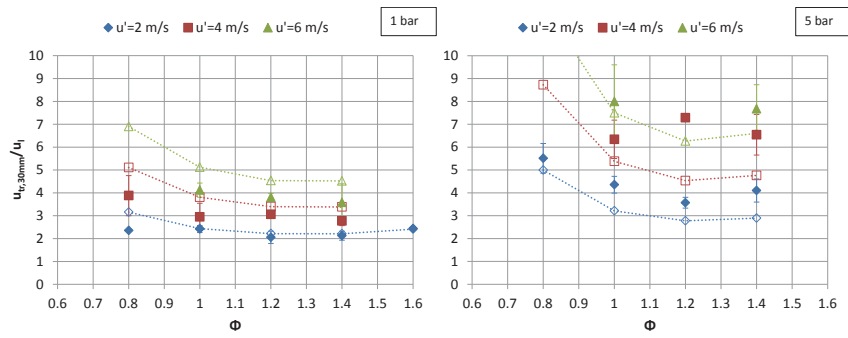


Figure 17: $u_{tr,30mm}/u_l$ vs. ϕ for the Peters model. Closed symbols - experiment, open symbols - model.

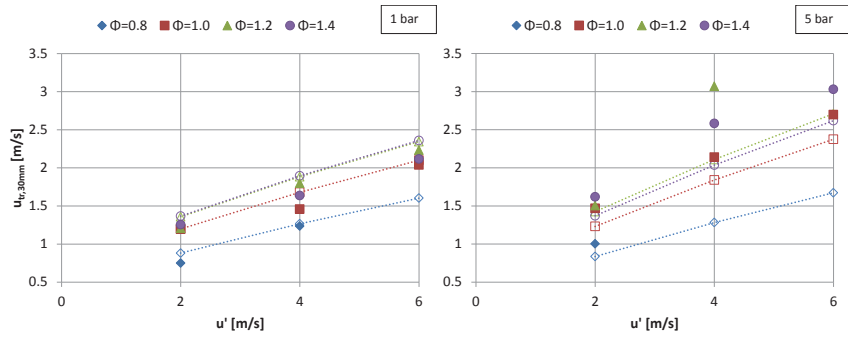


Figure 18: $u_{tr,30mm}$ vs. u' for the Zimont model. Closed symbols - experiment, open symbols - model.

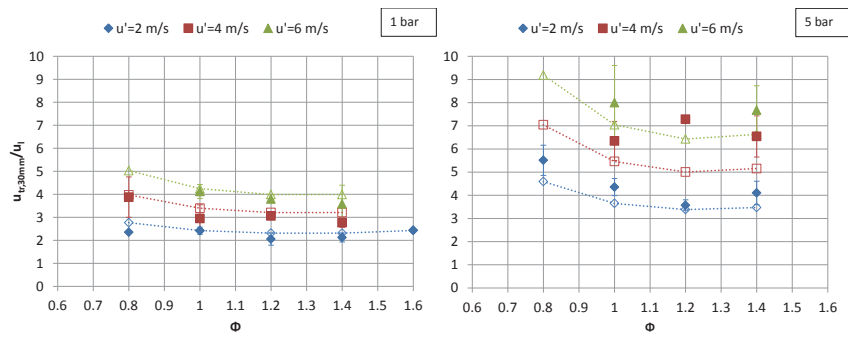


Figure 19: $u_{tr,30mm}/u_l$ vs. ϕ for the Zimont model. Closed symbols - experiment, open symbols - model.

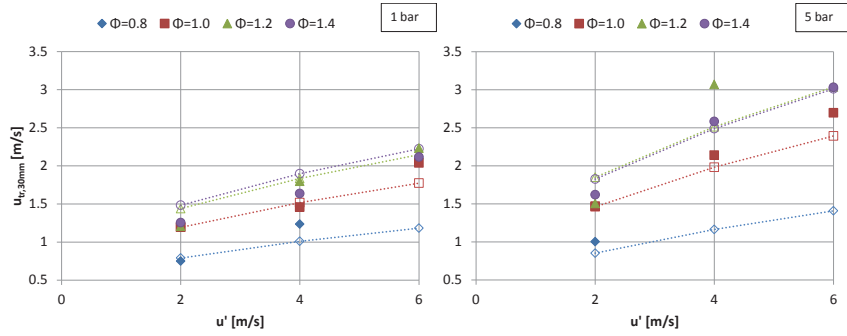


Figure 20: $u_{tr,30mm}$ vs. u' for the Dinkelacker model. Closed symbols - experiment, open symbols - model.

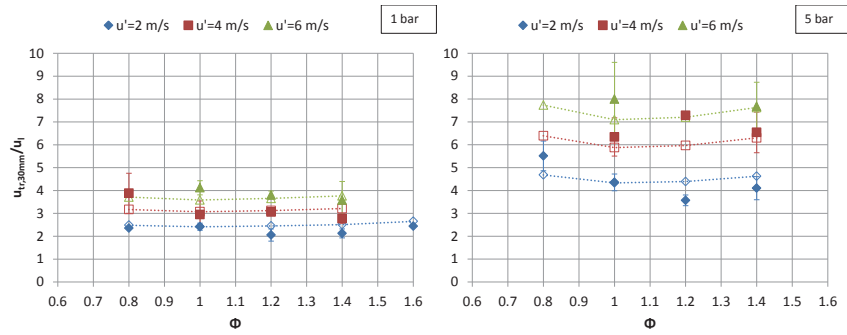


Figure 21: $u_{tr,30mm}/u_l$ vs. ϕ for the Dinkelacker model. Closed symbols - experiment, open symbols - model.

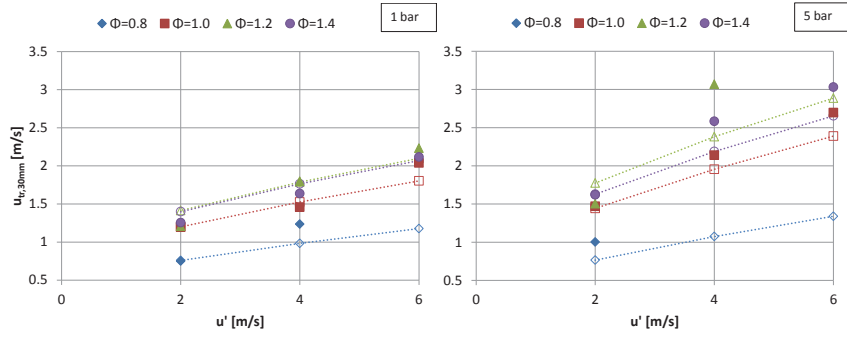


Figure 22: $u_{tr,30mm}$ vs. u' for the Kolla model. Closed symbols - experiment, open symbols - model.

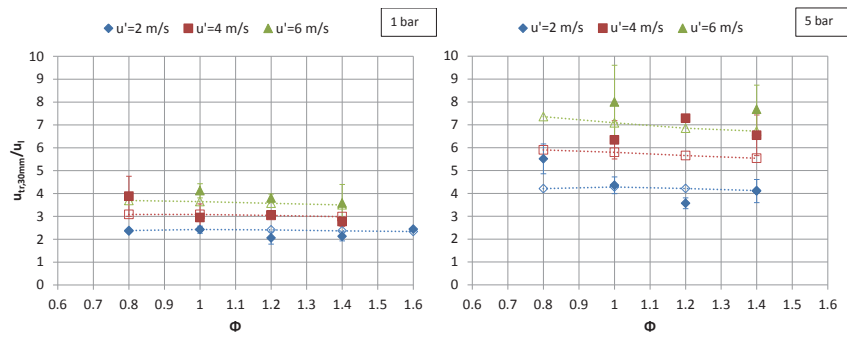


Figure 23: $u_{tr,30mm}/u_l$ vs. ϕ for the Kolla model. Closed symbols - experiment, open symbols - model.

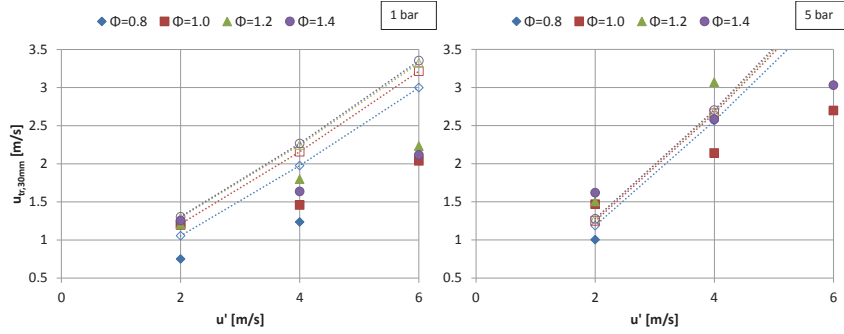


Figure 24: $u_{tr,30mm}$ vs. u' for the CFM with Γ according to Eqs. A.21 - A.26. Closed symbols - experiment, open symbols - model.

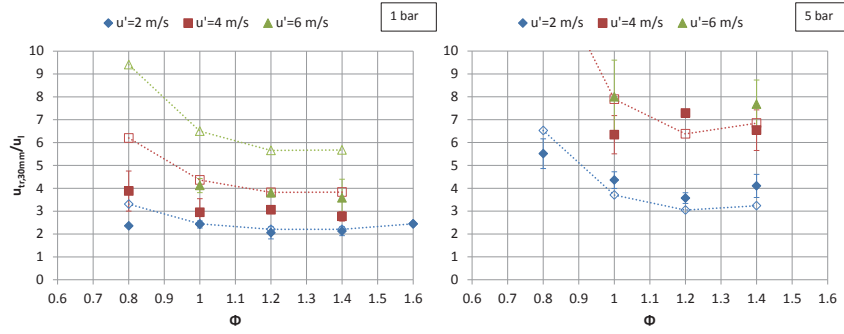


Figure 25: $u_{tr,30mm}/u_l$ vs. ϕ for the CFM with Γ according to Eqs. A.21 - A.26. Top - Methanol, bottom - ethanol. Closed symbols - experiment, open symbols - model.

550 Appendix A. Turbulent burning velocity models

Appendix A.1. Damköhler and derivatives

A large number of models assume the sole effect of turbulence to be flame front wrinkling leading to an increased flame area. Thus, the burning velocity ratio u_t/u_l is assumed to be equal to the flame surface area ratio A_t/A_l , where A_t is the wrinkled surface area and A_l is the mean, smooth flame surface area. Damköhler related this area ratio to the rms turbulent velocity divided by the laminar burning velocity:

$$\frac{A_t}{A_l} \sim \frac{u'}{u_l} \Rightarrow u_t \sim u' \quad (\text{A.1})$$

This expression is claimed to be valid for large u'/u_l . In many engine models the expression is changed to $u_t \sim u' + u_l$ to recover the laminar burning velocity when $u' \rightarrow 0$.

560 *Appendix A.2. Gülder*

Gülder derived the following expression for u_t [33, 19]

$$u_t = u_l + 0.6u'^{0.5}u_l^{0.5}Re_t^{0.25} \quad (\text{A.2})$$

565 Gülder later plotted $u_t/u_l - 1$ versus $(u'/u_l)^{0.5}Re_t^{0.25}$, where $Re_t = u'\Lambda/\nu$, for a large experimental dataset obtained from different research groups and obtained good approximation of the data with Equation A.2. Note that a large part of this dataset did not take into account the effects of flame stretch and instabilities on the laminar burning velocity.

Appendix A.3. Bradley et al.

570 Bradley et al. collected all known experimental values of turbulent burning velocities and searched for correlations on a theoretical basis using dimensionless terms describing the data set [34]. They developed a correlation in terms of the Lewis number Le and the Karlovitz stretch factor Ka , representing the dimensionless flow field strain.

$$u_t/u' = 0.88(KaLe)^{-0.3} \quad (\text{A.3})$$

575 where Ka was taken as $Ka = 0.157(u'/u_l)^2Re_t^{-0.5}$. The dependence of u_t/u' on the product $KaLe$ originated from the consideration of the effect of flame stretch on u_t , starting from the linear relation between flame speed and flame stretch for the local laminar flame [11].

Appendix A.4. Fractal-based models

580 Starting from Gouldin's suggestion of using a fractal geometry to describe the self-similar wrinkling of the flame front by the turbulence spectrum, Matthews et al. developed the following expression for the area increase [27, 28].

$$\frac{A_t}{A_l} = \left(\frac{L_{max}}{L_{min}}\right)^{D_3-2} \quad (\text{A.4})$$

L_{max} and L_{min} are the outer and inner cut-off of the wrinkling, D_3 is the fractal dimension of the flame surface. The ratio L_{max}/L_{min} is mostly set to the ratio of maximum to minimum turbulent length scale Λ/η_K [27, 35, 36].

585 The fractal dimension D_3 is given by Equation A.5 and describes the balance between turbulent flame wrinkling and laminar flame smoothing through flame propagation.

$$D_3 = 2.35\frac{u'}{u' + u_l} + 2.0\frac{u_l}{u' + u_l} \quad (\text{A.5})$$

Some authors account for the effect of stretch on the local flame speed by using the stretched laminar burning velocity u_n in their u_t model. u_n is then derived using a stretch model [30, 37, 29].

$$u_t = u_n \left(\frac{L_{max}}{L_{min}}\right)^{D_3-2} \quad (\text{A.6})$$

590 *Appendix A.5. Peters*

Peters derived an expression for the flame surface area increase due to turbulence using the G equation framework [25]. Considering a regime of highly turbulent combustion, with a thin reaction zone but thickened preheat zone through small scale eddy penetration, he obtained the following expression for u_t :

$$u_t = u_l + u' \left\{ -\frac{a_4 b_3^2}{2b_1} Da + \left[\left(\frac{a_4 b_3^2}{2b_1} Da \right)^2 + a_4 b_3^2 Da \right]^{1/2} \right\} \quad (\text{A.7})$$

595 Peters suggests the following values: $a_4 = 0.78$, $b_1 = 2.0$ and $b_3 = 1.0$.

Appendix A.6. Zimont/Lipatnikov

For the turbulent burning velocity u_t , Zimont suggested the following model:

$$u_t = Au' Da^{1/4} = Au' \left(\frac{\Lambda}{u' \tau_l} \right)^{1/4} \quad (\text{A.8})$$

600 where τ_l is a chemical time scale and A is a calibration constant with a suggested value of 0.5. The chemical time scale is based on the laminar flame thickness, using the molecular heat diffusivity D_t as the relevant diffusivity: $\tau_l = \delta_l / u_l = D_t / u_l^2$. The extended model of Lipatnikov and Chomiak with this expression for u_t has been validated against measurements in fan-stirred bombs, SI engines and several experimental databases [23].

Appendix A.7. Dinkelacker et al.

605 Dinkelacker et al. developed a turbulent burning velocity correlation based on a dataset measured by Kobayashi et al. of over 100 cone angles of bunsen flames for lean methane-, ethylene- and propane-air flames at operating pressures between 0.1-1.0 MPa [38]. They computationally estimated the flame cone angle using a 3D RANS simulation employing the common turbulent gradient diffusion approach for turbulent scalar transport and the following expression for the mean reaction source term \bar{w}_c :

$$\bar{w}_c = \rho_u u_l I_0 \Sigma \quad (\text{A.9})$$

The flame surface density Σ and stretch factor I_0 were directly modeled by an empirical expression for A_t/A_l :

$$\frac{A_t}{A_l} = \frac{u_t}{u_l} = 1 + a Re_t^{0.25} \left(\frac{u'}{u_l} \right)^b \left(\frac{p}{p_0} \right)^c \quad (\text{A.10})$$

615 The form of this correlation was inspired by the correlation of Gülder (see §Appendix A.2) and earlier work by Kobayashi et al. on the pressure dependence of turbulent burning velocity [39]. The constant a and exponents b and c were determined by numerical optimization comparing the experimental and calculated flame cone angles. Exponents b and c were found to be universal across fuels, whereas a was fuel dependent. A good

correlation was found between a and the Lewis number of the fuel-air mixture. The final correlation was:

$$\frac{u_t}{u_l} = 1 + \frac{0.46}{Le} Re_t^{0.25} \left(\frac{u'}{u_l} \right)^{0.3} \left(\frac{p}{p_0} \right)^{0.2} \quad (\text{A.11})$$

620 Inclusion of the Lewis number is reported to represent the effect of instabilities at low turbulence and that of stretch of the mainly positively curved leading edge of the flame brush.

Appendix A.8. Kolla et al.

625 Kolla et al. recently developed an expression for the leading edge turbulent burning velocity u_t using the Kolmogorov-Petrovskii-Piskunov (KPP) analysis [23, 40] in combination with their scalar dissipation rate model to close the mean reaction rate model:

$$\frac{u_t}{u_l} = \left\{ \frac{18C_\mu}{(2C_m - 1)\beta'} \left[[2K_c^* - \tau C_4] \left(\frac{u'\Lambda}{u_l \delta_l} \right) + \frac{2C_3}{3} \left(\frac{u'}{u_l} \right)^2 \right] \right\}^{1/2} \quad (\text{A.12})$$

The model constants in Equation A.12 were obtained using DNS data.

- C_m is typically 0.7
- 630 • K_c^* is related to the dilatation rate and is given by $K_c^* \simeq 0.85\tau$ where τ is a heat release parameter given by $\tau = (T_{ad} - T_u)/T_u$
- β' represents the flamelet curvature contribution and its value is 6.7
- C_3 and C_4 represent turbulence-scalar interaction effects and depend on the Karlovitz number Ka

$$Ka = \left(\frac{\nu_u}{u_l \eta_K} \right)^2 = \left([2(1 + \tau)^{0.7}]^{-1} \left(\frac{u'}{u_l} \right)^3 \left(\frac{\delta_l}{\Lambda} \right) \right)^{0.5} \quad (\text{A.13})$$

$$C_3 = \frac{1.5 \sqrt{Ka}}{1 + \sqrt{Ka}} \quad (\text{A.14})$$

$$C_4 = 1.1(1 + Ka)^{-0.4} \quad (\text{A.15})$$

635 Appendix A.9. Coherent Flame Model

As stated by Driscoll, turbulent flame wrinkling is a geometry dependent process and has a memory of upstream locations [15]. Coherent Flame Models (CFM) are a class of models that implement this observation by solving a transport equation for the temporal and spatial evolution of the flame surface density Σ [15, 26, 41]. The general form of this equation is usually as follows:

$$\frac{d\Sigma}{dt} + \frac{\partial u_i \Sigma}{\partial x_i} = \frac{\partial}{\partial x_i} \left(\frac{\nu_t}{\sigma_c} \frac{\partial \Sigma}{\partial x_i} \right) + S - M - Q \quad (\text{A.16})$$

The two terms on the left hand side represent the convection of wrinkledness to downstream locations. The first term on the right hand side simulates the spreading of the flame brush due to turbulent diffusion. The three other terms on the right hand side respectively represent the source term for flame surface density, the mean merging rate of flame surface and the mean flame front quenching rate. Many models have been proposed for these three terms [41, 15]. The model is an analytical formulation of a turbulent flame consisting of coherent laminar flame elements (flamelets), where by coherent, it is implied that a local laminar flamelet retains its identity although it is severely distorted and strained by the turbulent motions.

Richard et al. have recently reduced their 3D CFM model to a formulation that is compatible with quasi-dimensional engine modeling [26]. The mass burning rate was given by:

$$\dot{m}_b = \rho_u u_l A_l \Sigma \quad (\text{A.17})$$

where A_l is the mean, smooth flame front surface and Σ is the flame surface density, of which the temporal evolution is described by the following balance equation.

$$\frac{1}{\Sigma} \frac{d\Sigma}{dt} = \Gamma(u'/u_l, \Lambda/\delta_l) \frac{u'}{\Lambda} \left(\frac{\Sigma_{eq} - \Sigma}{\Sigma_{eq} - 1} \right) - \frac{2}{r_{bg}} (1 + \tau)(\Sigma - 1)u_l \quad (\text{A.18})$$

where $\tau = \rho_u/\rho_b$, $r_{bg} = (3V_b/4\pi)^{1/3}$ is the burnt gas mean radius and the laminar flame thickness δ_l is computed according to $\delta_l = \nu/u_l$. The stretch efficiency function Γ measures the efficiency of turbulence motions to wrinkle the flame front. The first term on the right hand side represents the flame strain caused by all turbulent structures, while the second simulates the effect of thermal expansion, which limits the flame front wrinkling by imposing positive curvature on the flame front [26]. Σ_{eq} is the value of Σ when equilibrium is reached between turbulence and flame front wrinkling. It is given by:

$$\Sigma_{eq} = 1 + \frac{2}{u_l} \sqrt{\frac{C\Gamma u'^2}{1 - C^*/(1 + \tau)}} \quad (\text{A.19})$$

Where proposed values for the constants are $C^*=0.5$ and $C=0.12$. Richard et al. [26] report that the use of a balance equation for Σ improves the transition from laminar to turbulent combustion compared to fractal modeling approaches such as that by Bozza et al. [35]. Here, this equation is solved between spark time and the experimental time for which the burned gas radius $r_b=0.03$ m (t_{30mm}), with the assumption of constant u' and a quadratic evolution of r_b .

$$r_b(t) = \frac{0.03}{t_{30mm}^2} \cdot t^2 \quad (\text{A.20})$$

The stretch efficiency function Γ is mainly a function of the integral length scale and the laminar flame thickness, and is nearly independent from the rms turbulent burning velocity u' [15]. Charlette et al. obtained an expression for $\Gamma(u'/u_l, \Lambda/\delta_l, Re_t)$ from

spectral analysis of DNS simulation of single vortex-flame interactions [42]:

$$\Gamma = [(f_u^{-a} + f_\Lambda^{-a})^{-1/a}]^{-b} + f_{Re}^{-b}]^{-1/b} \quad (\text{A.21})$$

$$f_u = 4 \left(\frac{27C_k}{110} \right)^{1/2} \left(\frac{18C_k}{55} \right) \left(\frac{u'}{u_i} \right)^2 \quad (\text{A.22})$$

$$f_\Lambda = \left[\frac{27C_k \Pi^{4/3}}{110} \cdot \left(\left(\frac{\Lambda}{\delta_l} \right)^{4/3} - 1 \right) \right]^{1/2} \quad (\text{A.23})$$

$$f_{Re} = \left[\frac{9}{55} \exp \left[-\frac{3}{2} C_k \Pi^{4/3} Re_i^{-1} \right] \right]^{1/2} \cdot Re_i^{1/2} \quad (\text{A.24})$$

$$a = 0.60 + 0.20 \exp[-0.1(u'/u_i)] - 0.20 \exp[-0.01(\Lambda/\delta_l)] \quad (\text{A.25})$$

$$b = 1.4 \quad (\text{A.26})$$

The turbulent burning velocity of methanol-air mixtures

J. Vancoillie^a, G. Sharpe^b, M. Lawes^b, S. Verhelst^a

^a*Department of Flow, Heat and Combustion Mechanics, Ghent University
Sint-Pietersnieuwstraat 41 B-9000 Gent, Belgium*

^b*School of Mechanical Engineering, University of Leeds
Leeds LS2 9JT, UK*

5

Abstract

Methanol is a sustainable and versatile alternative fuel for spark-ignition engines and other combustion applications. To characterize the combustion behavior of this fuel, a good understanding of the factors affecting its turbulent burning velocity is required. This paper presents experimental values of the turbulent burning velocity of methanol-air mixtures obtained in a fan-stirred bomb, for $u' = 2-6$ m/s, $\phi = 0.8-1.4$, $T = 358$ K and pressures up to 0.5 MPa. In combination with laminar burning velocity values previously obtained on the same rig, these measurements are used to provide better insight into the various factors affecting u_t of methanol, and to assess to what degree existing turbulent combustion models can reproduce experimental trends. It appeared that most models correctly accounted for the effects of turbulent rms velocity u' . With respect to the effects of ϕ and pressure, however, models accounting for flame stretch and instabilities, through the inclusion of model terms depending on thermodynamic mixture properties and pressure, had a slight edge on simpler formulations.

Keywords: methanol, spark-ignition engine, thermodynamic, modeling, turbulent burning velocity, constant volume bomb

1. Introduction

The use of light alcohols as spark-ignition engine fuels can help to increase energy security and offers the prospect of carbon neutral transport. Compared to other alternatives, such as hydrogen or battery-electric vehicles, liquid alcohols entail less issues regarding fueling and distribution infrastructure and are easily stored in a vehicle. In addition, the properties of these fuels enable considerable improvements in engine performance and efficiency as several investigations on converted gasoline engines have demonstrated [1].

In addition to bio-ethanol, methanol is interesting since it is versatile from a production point-of-view. Biofuels can only constitute part of our energy supply because of the limited area of arable land [2, 3]. Methanol, on the other hand, can be produced from a wide variety of renewable (e.g. gasification of wood, agricultural by-products and municipal waste) and alternative fossil fuel-based feed stocks (e.g. coal and natural

*Corresponding author. Tel.: +32(0)92643306; Fax: +32(0)92643590
Email address: sebastian.verhelst@ugent.be (S. Verhelst^a)
Preprint submitted to Elsevier

gas). A sustainable closed-carbon cycle where methanol is synthesized from renewable hydrogen and atmospheric CO₂ has been proposed [4].

To characterize the combustion behavior of methanol-air mixtures in practical applications, data for the laminar burning velocity are needed, together with a good understanding of the factors affecting turbulent burning velocities. The laminar burning velocity of methanol-air mixtures has been studied by the current authors in previous work [5, 6, 7, 8]. Turbulent burning velocity data for methanol-air mixtures are scarce, and difficult to compare due to reasons associated with the definition of the turbulent burning velocity as well as its dependency on experimental techniques and rigs [9].

This paper presents experimental values of the turbulent burning velocity of methanol-air mixtures measured during spherical explosions in a fan-stirred bomb. Measurements were made at rms turbulent burning velocities u' between 2 and 6 m/s, equivalence ratios between 0.8 and 1.4, pressures up to 0.5 MPa and at an initial temperature of 358 K. Next to obtaining better understanding of the different parameters affecting the burning velocity, an additional objective of this study was to assess to what degree the different models proposed in the literature can reproduce the trends observed over the full range of conditions investigated here. Therefore, comparisons have been made with data derived using several widely used turbulent burning velocity correlations.

2. Experimental methods

2.1. The Leeds Mk II combustion vessel

The turbulent burning velocity was measured using the spherically expanding flame technique. The experiments were performed in the Mk II high pressure fan-stirred combustion vessel at Leeds University. The details of the experimental apparatus have been extensively described in [10]. The spherical, stainless steel vessel has a 380 mm inner diameter and is capable of withstanding temperatures and pressures generated from explosions with initial pressures up to 1.5 MPa and initial temperatures up to 600 K [11]. The vessel is equipped with three pairs of orthogonal windows of diameter 150 mm. An electric heater at the wall provided up to 2 kW for preheating the vessel and mixture up to 358 K. Gas temperatures were obtained from a sheathed type-K thermocouple. Pressures were measured during the explosion with a Kistler type 701A pressure transducer. A central spark plug was used with ignition energies of about 23 mJ, supplied from a 12V transistorized automotive ignition coil. The spark gap was set to 1.2 mm for all present experiments.

Turbulence was generated in the vessel by four identical eight bladed fans in a regular tetrahedron configuration. These were also used to mix the reactants. The fans were directly coupled to electric motors with separate speed controllers. Each fan was separately adjustable between 200 and 10,000 rpm. The speed of individual fans was maintained within 5% of each other and adjusted to attain the required turbulence intensity. The rms turbulent velocity and integral length scale have been determined using Laser-Doppler Velocimetry (LDV) [9]. In the central, optically accessible region of the vessel, a reasonably uniform isotropic turbulence was found with u' given by Equation 1.

$$u'(\text{m/s}) = 0.00119f_s(\text{rpm}) \quad (1)$$

Where f_s is the fan speed in rpm. The estimated maximum deviation of u' from this equation is 10%. From a two-point correlation using a second LDV system the integral length scale Λ was found to be 0.02 ± 0.001 m and was independent of all operating variables from 1000 to 10,000 rpm.

2.2. Schlieren flame photography

Following central spark ignition, the growth rate of spherically expanding flames was studied by high speed schlieren cine photography. This is a well established method for flame imaging in combustion studies at Leeds University [12, 13]. A high speed Phantom digital camera with 256 megabytes integral image memory was used to capture flame propagation. The camera speed was between 5000 and 10,000 frames/s with 384 x 384 pixels, the resolution was 0.4065 mm/pixel. At small flame radii the measured flame speed is very sensitive to determination of the flame radius from the digital images [14]. However, at these radii, the flame speed is affected by spark effects [10]. It was therefore decided to sacrifice spatial resolution at small radii in favor of higher frame rate and visibility of the entire vessel window area. In order to determine the turbulent burning velocity, image processing techniques were employed to automatically and robustly detect and reconstruct the flame front based on the maximum grayness gradient in the schlieren images.

Due to the turbulent flame brush thickness, a problem particular to turbulent burning velocity measurements is the choice of the flame front surface to evaluate the burning velocity. This choice can affect the burning velocity by a factor up to 4 [15, 16]. This is shown diagrammatically in Figure 1. For a general spherical radius R_j , between the flame root radius R_r and the flame tip radius R_t , there will be a certain mass of unburned gas m_{ui} and burned gas m_{bi} within that sphere, but outside the sphere of radius R_r . Similarly, outside a sphere of that radius, but within a radius of r_t , there will be a mass of unburned gas m_{uo} and burned gas m_{bo} .

In order to quantify the influence of the selected flame front surface on the burning velocities obtained in the present rig, Bradley et al. performed simultaneous high speed photography of images from schlieren and laser sheet Mie scattering during spherical explosions [17]. This work yielded radial distributions of the progress variable \bar{c} , extending from a value of $\bar{c} = 0$ at R_r , to $\bar{c} = 1.0$ at R_r . An important result from their study is that for a certain radius r_v , at which the total volume of unburned gas inside the sphere is equal to the total volume of burned gas outside it, the associated turbulent burning velocity, u_{tv} is given by the following simple expression:

$$u_{tv} = \frac{\rho_b}{\rho_u} \frac{dr_v}{dt} \quad (2)$$

In the present study, this basic expression was used to obtain u_t from the schlieren images. It was assumed that the radius R_{sch} , where the projected surface area of unburned gas inside it was equal to the projected surface area of burned gas outside it, was in fact r_v . The work of Bradley et al. also yielded an empirical expression to relate this burning velocity to the turbulent velocity associated with the production of burned gas u_{tr} . This expression has been used throughout the rest of this work.

$$u_{tr} = 0.9 \frac{\rho_b}{\rho_u} \frac{dR_{sch}}{dt} \quad (3)$$

2.3. Mixture preparation

Before an explosion, the vessel was first flushed with dry air to remove most of the residuals from a previous experiment, after which it was evacuated down to 0.03 bar, filled with dry air to atmospheric pressure, and evacuated again to less than 0.03 bar. The liquid methanol volume to be injected into the bomb was found from the required molar mixture composition, the liquid methanol density and the known volume of the bomb. Liquid methanol was injected with a calibrated gas tight syringe, through a needle valve. Four syringes were employed, in this study, with volumes of 5, 10, 25 and 50 cm³, depending upon the volume of fuel required. Injection was carried out under vacuum at 0.03 bar and a temperature of 10-20 K higher than the ignition temperature, which aided methanol vaporization.

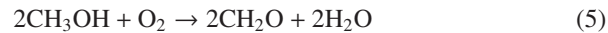
After injection the partial pressure and temperature of methanol vapor was measured in order to compare it with the theoretically required value resulting from the assumption of ideal gases. Next, the vessel was filled with dry air to the required initial pressure. Only conditions with the vapor pressure of methanol below the saturation pressure were studied here.

The mixture temperature was controlled by a CAL320PID controller in combination with a 2 kW electrical heater. As the heater coil is mounted inside the vessel, in contact with the mixture, it proved important to switch the heater off at least two minutes before injection and to leave it off till ignition. Failing to do so resulted in dissociation and partial oxidation of the methanol fuel, leading to low experimental repeatability. The chemical reactions at play are believed to be the following:

- In the absence of air (partial vacuum) the methanol can dissociate to formaldehyde and hydrogen. This reaction is associated with a large increase in partial pressure and can lead to burning velocities two to threefold the expected value, an effect of the high burning velocities of H₂ [18].



- When enough air is present (during filling with dry air) a partial oxidation of the methanol-air mixture can occur. This would lead to a mild increase in partial pressure (molar ratio of 4/3 between products and reactants) and a reduction in burning velocity due to the non-reactive water vapor.



When the heater is left on, the temperature in the vicinity of the heater coil will be a lot higher than the average mixture temperature so that these reactions can indeed be triggered.

3. Repeatability

At least three explosions were performed at each condition to obtain a measure for the repeatability of the experiments and to capture the stochastic variation associated with turbulent tests. In between experiments, the recorded pressure traces were used to quickly assess the repeatability by ensuring there was less than 5% variation in the time to reach a pressure rise of 50%. After processing the images, the standard deviation on the turbulent burning velocity was calculated as a function of flame radius for each condition.

The principal uncertainty was in making up the mixture. Therefore, factors affecting mixture stoichiometry were accurately controlled.

- The consistency of pressure and temperature just prior to ignition was of importance. The tolerance for these parameters was set at ± 0.02 bar and ± 3 K respectively.
- Residuals were considered as another source affecting mixture composition, but were kept at a minimum through adequate flushing of the vessel after each experiment.
- The hygroscopic nature of methanol could affect the fuel purity. Therefore, methanol was stored in small 50 ml flasks, minimizing the contact with ambient air. The water content of methanol stored in such a way during the entire course of this work was checked and proved to be below 1 % by mass.
- Another factor was the uncertainty of the full scale deflection of the syringe used to inject methanol. The manufacturer tolerance was given as 0.5 % at full scale. This would correspond to an average uncertainty on the equivalence ratio of below 1.5 % [13].
- A final influence was the vessel sealing. Although the seals were replaced during the initial stages of this work, still some degree of leakage was present. This is particularly important for the measurements at elevated pressures. At these conditions part of the methanol-air mixture leaks during the addition of dry air, which affects stoichiometry. The leakage rate was estimated by measuring the rate of pressure decrease after the vessel had been pressurized to 5 bar and was in the order of 0.01 bar per minute. Pressurizing the vessel took around 3 minutes. The worst case effect on ϕ , assuming that all leakage consists of fuel vapor and the leakage is at its maximal rate throughout the pressurization, is below 5%.

Although the mixture stoichiometry was controlled by injecting a known amount of methanol, the correct composition of the mixture was cross-checked by comparing measured partial pressures of methanol vapor to the theoretical value assuming ideal gas behavior.

It appeared that the measured partial pressure of methanol vapor was consistently 5-10 % lower than the theoretical value, which means the actual mixture equivalence ratio was lower than the desired value by the same percentage. This was found to be due to fuel absorption on carbon deposits in the vessel's seal cavities. Most models

195 predict the turbulent burning velocity based on the laminar burning velocity at the same conditions. Since the laminar burning velocity values used in this work were measured using the same setup [8] and consequently suffer from a similar divergence in ϕ , the divergence should have no effect on the qualitative trends predicted by the models. In the following, the results are therefore presented as function of the desired value of ϕ and not as function of the correct ϕ based on partial pressure, as was done in [8].

4. Measurement conditions

200 Turbulent methanol-air flames were measured at two pressures (1 and 5 bar), five desired equivalence ratios ($\phi=0.8, 1.0, 1.2, 1.4, 1.6$) and three rms turbulent velocities ($u' = 2, 4, 6$ m/s). All measurements were done at 358 K. Table 1 lists the measurement conditions. Table 2 summarizes the mixture Lewis number Le , measured laminar burning velocity u_l and Markstein length L_b measured at the same conditions. These values are discussed in more detail in [8].

205 For some conditions, marked by * in Table 1, less than 3 repetitions were performed, so the results should be handled with care. For lean mixtures, flame quenching can occur at elevated values of u' . This is marked by a 'q' in the table.

5. Observations of spherically propagating turbulent methanol flames

210 Shown in Figure 2 are schlieren images of stoichiometric methanol-air flames ($\phi=1.0$) as a function of time after ignition, for different initial pressures and u' . Figure 3 shows the same for a rich mixture ($\phi=1.4$). For each measurement condition, multiple experiments were conducted and one representative experiment is shown in the figures. Both figures show how the wrinkling of turbulent flames increases with u' , resulting in a faster flame propagation.

215 The flames at 1 bar and elevated turbulence ($u'=6$ m/s) are heavily distorted and convected away from the spark gap. This decreases the accuracy of representing flames as expanding spherically from the point of ignition. Explosions at elevated pressure ($p=5$ bar) show that not only the centroid of the flame is closer to the spark gap, but flames are more spherical in appearance. Mansour suggests that the amount of flame distortion is related to the Markstein number. Flames with higher positive Ma at high u' are locally slower and consequently more distorted and partially quenched, as illustrated in Figure 2 ($p=1$ bar, $u'=6$ m/s).

220 The same Markstein number effect might explain why the rich methanol flames seem to cope better with turbulence. For comparable conditions, the rich turbulent flames ($\phi=1.4$; $L_b=0.55$ mm at 1 bar, -0.26 mm at 5 bar) propagate faster and less distorted than the stoichiometric flames ($\phi=1.0$; $L_b=0.85$ mm at 1 bar, 0.05 mm at 5 bar) although their laminar burning velocity is lower. A faster turbulent flame speed in spite of reduced u_l also applies when comparing the results at elevated pressure to those at 1 bar. The lower Markstein number at 5 bar leads to less reduction in local flame speed due to stretch. Additionally, the inherent laminar instability of rich flames at elevated pressures can produce a more finely wrinkled flame, further increasing the turbulent flame speed.

6. Turbulent burning velocities versus radius

Figure 4 shows the turbulent mass burning velocity u_{tr} (according to Eq. 3) plotted as a function of mean schlieren radius r_{sch} . Figure 4 illustrates the influence of u' at different equivalence ratios. A first thing to notice is that after an initial period of spark affected flame propagation ($r_{sch} < 10$ mm) u_{tr} rises as the flame radius grows. This well known phenomenon arises because, in the early stage of flame propagation, the flame can only be wrinkled by length scales less than the size of the flame kernel [16]. As a consequence, the rms turbulent burning velocity effective in wrinkling the flame front, u'_k , is less than the value measured in the bomb in the absence of any flame (u') [16].

Two obvious trends can be identified from Figure 4. The first is that u_{tr} obviously increases with u' through more intense flame front wrinkling. As the turbulence intensity rises, so does the stochastic variation on u_{tr} . Mansour attributes this to the increasing importance of merging and quenching effects, and the associated distortion in spherical flame front shape, at higher values of u' [13]. A second trend is that the turbulent burning velocity grows with pressure, especially for rich mixtures, despite a decreased laminar burning velocity. As mentioned before, this can be attributed to lower Markstein numbers and the effects of preferential diffusion and flame instabilities.

7. Qualitative trends

To distinguish qualitative trends of turbulent burning velocity as a function of u' , ϕ and p , and to quantitatively compare the experimental values of u_{tr} to model predictions, the flame velocity at a fixed mean flame radius of 30 mm was selected to provide a single representative value of u_{tr} . This radius is large enough to discount any spark effects and is small enough to ensure that most flames grew to this radius before parts of the flame edge extended beyond the window due to bulk flame convection effects [9].

Figure 5 plots the turbulent burning velocity at 30 mm ($u_{tr,30mm}$) versus rms velocity u' for methanol-air flames at 1 and 5 bar. It is clear that the turbulent burning velocities can be well approximated by a linear correlation with u' , with some slight downward bending.

In Figure 6 the same results are replotted as $u_{tr,30mm}$ normalized by u_l versus the ratio of u' to u_l . Linear fits are also shown. Whereas Verhelst reported an almost perfect fit very close to $u_{tr,30mm} = u' + u_l$ for hydrogen-air flames, this is not the case for the current results [19]. This can be partly due to the experimental uncertainty on $u_{tr,30mm}$ and u_l , but also indicates that for alcohol-air flames at these conditions, factors other than u_l and u' are important to the turbulent flame development.

To further illustrate this, Figure 7 shows the turbulent burning velocity ratio $u_{tr,30mm}/u_l$ as a function of equivalence ratio ϕ . The ratio $u_{tr,30mm}/u_l$ can be seen to remain fairly constant with equivalence ratio. At 5 bar, there is a slight rise for the leanest and richest mixtures. The figures also confirm that $u_{tr,30mm}/u_l$ rises as the pressure increases. These two observations are in line with the differential diffusion theory [20]. As the molecular weight of methanol is the same as that of O_2 ($M=32$ g/mol), its molecular

275 diffusivity will be comparable. This means the Lewis number will be largely independent of ϕ and the effects of preferential diffusion are limited. Note that the present results for methanol at 5 bar, $u'=2$ m/s correspond well to the values of Lawes et al [21], especially **when keeping** in mind that the real ϕ is 5-10% lower than the desired ϕ displayed here.

280 8. Model comparison

8.1. Model implementation and calibration

The turbulent methanol-air measurements described above are used to evaluate the predictive capabilities of several turbulent burning velocity models. The unburned gas mixture properties used in the model equations (e.g. ν , ρ_u) were calculated using a thermodynamic database [22]. The laminar burning velocities and Lewis numbers of the different mixtures are summarized in Table 2. An assumption in various models, $u' \gg u_l$, is generally satisfied here.

Numerous models and correlations exist to predict the turbulent burning velocity and unfortunately no single model has emerged as the most accurate or most widely applicable. For this work, a selection is made of models that have been widely demonstrated and used in simulation of SI engines or other combustion applications. Lipatnikov and Chomiak [23] tested a variety of models and concluded that only a few expressions can predict all the experimental trends they observed in the body of literature: those of Zimont/Lipatnikov [24, 23], Peters [25] and the Coherent Flame Model (CFM) [26]. Fractal-based models [27, 28] were reported to reproduce many trends.

285 These and other models used in this work are described in the Appendix and the corresponding original references. The model formulations are slightly adapted here to correspond to the way they would be used in a combustion simulation code. This involved adding a calibration factor C_2 and a term u_n to ensure the stretched laminar burning velocity u_n appears when $u' \rightarrow 0$. The expressions are used here to directly calculate the mass consumption velocity u_{tr} .

- Damköhler:

$$u_t = C_2 u' + u_n \quad (6)$$

- Gülder:

$$u_t = 0.6 C_2 u'^{0.5} u_n^{0.5} Re_t^{0.25} + u_n \quad (7)$$

- Bradley $KaLe$:

$$u_t = 0.88 C_2 u' (KaLe)^{-0.3} + u_n \quad (8)$$

- 305 • Bradley $KaMa$:

$$u_t = 0.54 C_2 \alpha (Ka)^\beta + u_n \quad (9)$$

- Fractals:

$$u_t = u_n (Re_t)^{0.75(D_3-2)} \quad (10)$$

$$D_3 = \frac{2.35 C_2 u'}{u' + u_n} + \frac{2.0 u_n}{u' + u_n} \quad (11)$$

- Peters:

$$u_t = 0.195C_2u'Da \left[\left(1 + \frac{30.52}{Da} \right)^{0.5} - 1 \right] + u_n \quad (12)$$

- Zimont:

$$u_t = C_2u'Da^{1/4} + u_n \quad (13)$$

- Dinkelacker:

$$u_t = u_n + \frac{0.46C_2 \cdot u_n}{Le} Re_i^{0.25} \left(\frac{u'}{u_n} \right)^{0.3} \left(\frac{p}{p_0} \right)^{0.2} \quad (14)$$

310

- Kolla:

$$\frac{u_t}{u_l} = \left\{ \frac{18C_2}{(2C_m - 1)\beta'} \left[[2K_c^* - \tau C_4] \left(\frac{u'\Lambda}{u_l\delta_l} \right) + \frac{2C_3}{3} \left(\frac{u'}{u_l} \right)^2 \right] \right\}^{1/2} \quad (15)$$

- Coherent Flame Model: this model is used in its original form with the fitted function for Γ represented by Equations A.21 - A.26. For this choice of Γ the model is calibrated by varying the constant C in Equation A.19.

As **mentioned above**, only part of the turbulent spectrum is effective in wrinkling the flame. To account for this flame development, the effective rms turbulent burning velocity u'_k is used instead of u' in the model formulations. Bradley et al. developed an expression for u'_k based on a large experimental dataset and the integration of the power spectral densities of eddies inside the bomb between the Kolmogorov scale and a limiting scale in the bomb [16]. The value for u'_k is calculated based on this work. For the Coherent Flame Model, the temporal development of flame wrinkling is implemented by solving the balance equation for the flame surface density Σ (Eq. A.18). The calibration constants are chosen in such a way that the model prediction exactly matches the measured burning velocity $u_{tr,30mm}$ at 1 bar, $\phi=1.0$ and $u'=2$ m/s.

8.2. Model comparison

In what follows, the turbulent burning velocity models are tested for varying rms turbulent velocity and varying equivalence ratio. The results are displayed in terms of $u_{tr,30mm}$ vs. u' and $u_{tr,30mm}/u_l$ vs ϕ plots. Experimental results are marked by the closed symbols, while the open symbols represent model results. A selection of the most promising models is made at the end of this section. The models' performance is demonstrated using some selected plots. Further modeling results can be found in Electronic Supplementary Material.

8.2.1. Damköhler

As could be expected from the model equations, Figure 8 illustrates that the predicted trend for u_t versus u' is linear, leading to an overprediction of u_t at high values of u' . The results for u_t/u_l show good correspondence for stoichiometric to rich mixtures (Figure 9). For lean mixtures, the simulated ratio u_t/u_l is too high, probably because the calculated u_t is primarily defined by u' at those conditions (see Eq. 6). The results

suggest that the effects of pressure on u_t/u_l are not well represented by the Damköhler model. The results for the Peters model are very similar (not shown here), which could be expected since both models are the same in the limit for large Damköhler numbers [12].

8.2.2. Gülder

The model equations of Gülder correctly reproduce the bending of the u_t vs. u' curve (see Figure 10). The evolution of u_t/u_l with ϕ is well predicted by the Gülder model (Figure 11). The underprediction of the effect of pressure on u_t/u_l is less pronounced than for the Damköhler model.

8.2.3. Bradley

The $KaLe$ correlation of Bradley et al. also reproduces the bending of the u_t vs. u' curve (not shown here). The u_t/u_l vs. ϕ evolution is well predicted, except maybe for the richest mixtures, where there is a slight underestimation (see Figure 13). The results illustrate a striking underestimation of the effect of pressure on u_t/u_l (see Figure 13). This is possibly due to the insensitivity of the Lewis number to pressure. Note that the effect of this underestimation on the predicted u_t will be lower at elevated, engine-like pressures, because u_l varies only slightly with pressure at these conditions.

To introduce the effect of pressure on flame dynamics, Bradley et al. [16] recently proposed a correlation for u_t/u' as a function of Ka and Ma_{sr} based on spherical explosions and twin kernel implosions in a fan-stirred bomb of ethanol-air mixtures for a wide range of ϕ , p and u' . The correlation reflects that, at constant Ka , there is an increased rate of burning in laminar flamelets, independent of that due to wrinkling, as Ma_{sr} is decreased in the predominantly positively stretched flames. At higher Ka , flame front merging and extinction lead to a decrease in u_t/u' .

8.2.4. Fractals

The fractal model underestimates the slope of the u_t vs. u' curve, especially at higher pressures (Figure 14). This model does not reproduce the rise in u_t/u_l for rich mixtures, as becomes clear from Figure 15. Also, it gives the worst underestimation of the effect of pressure on u_t/u_l among the models considered here. It was attempted to include the effect of stretch on the local burning velocity u_n by applying the stretch submodels of both Teraji et al. [29] and Chung & Law [30, 31]. The model of Teraji et al. did not enable any significant improvements. That of Chung & Law is only valid for small values of Ka and produced negative values of u_t for the highly turbulent flames considered here.

8.2.5. Zimont

The trends predicted by the model of Zimont agree well with those observed experimentally (see Figures 18 and 19). For the richest mixtures, there is a slight underprediction of u_t/u_l , but the representation of the pressure effect on u_t/u_l is one of the best among the models considered here. The model of Kerstein [32] was also evaluated and as suggested by Lipatnikov and Chomiak, its performance is very close to that of the Zimont model [23] (not shown here).

8.2.6. Dinkelacker

380 As can be seen in Figures 20 and 21 the predictive performance of the Dinkelacker model in terms of equivalence ratio and pressure is very good. The inclusion of a pressure dependent term in Equation 14 leads to the best representation of the pressure effect among the models evaluated here.

8.2.7. Kolla

385 The model of Kolla et al. performs rather poorly (see Figures 22 and 23). The bending of the u_t vs. u' curve is reproduced but the slope of the curve is underestimated. Also, u_t/u_l is predicted to be insensitive to equivalence ratio, which is in disagreement with the experimental results.

8.2.8. Coherent Flame Model

390 Figures 24 and 25 display the Coherent Flame model performance for Γ according to Eqs. A.21 - A.26. The slope of the u_t vs u' curve is too high. This is an indication that the model equations do not correctly reproduce the flame development as encountered in the spherical flames. The use of the effective rms turbulent velocity u'_k in these equations improves the correspondence to experiments (not shown here).

395 The effect of pressure on u_t is mainly implemented through the dependence of Γ on laminar flame thickness δ_l . The stretch efficiency function was derived for engine-like, high pressure conditions. At the moderate pressure conditions considered here, δ_l varies significantly with pressure, which might explain the exaggerated response of u_t to pressure.

400 The effect of equivalence ratio on u_t/u_l is well reproduced for stoichiometric and rich mixtures, but heavily overestimated u_t/u_l at lean conditions. Possibly this is due to the fact that Γ was primarily fitted to results obtained for stoichiometric flames.

8.3. Conclusions

405 In the current work, the turbulent combustion behavior of methanol was evaluated based on turbulent burning velocity measurements obtained in a fan-stirred bomb. The results indicate that the effect of rms turbulent velocity u' on u_t is well represented by most models. It is slightly underestimated by the Fractals and Kolla model, and considerably overestimated by the CFM model. The models of Dinkelacker, Zimont, Bradley *KaLe* and Gülder perform best as they reproduce the effects of varying
410 ϕ through the inclusion of thermodiffusive mixture properties. For most models there was an underprediction of the effect of pressure on u_t . The thermodiffusive properties in these models do not depend on pressure and consequently cannot reflect the effects of reduced flame stretch effects and increased flame wrinkling at higher pressures. The Dinkelacker model performed best in this respect through the inclusion of a pressure
415 dependent term in the model formulation. The Coherent Flame Model arguably performed the worst among the models considered here. Possibly this is because the model was developed with the explicit goal of engine simulations in mind and its direct dependence on flame thickness is not valid at the moderate pressures during bomb experiments. Future model developments should focus on reproducing the effects of
420 pressure on the flame phenomenology. One approach could be to include measured Markstein numbers, which depend on pressure, in the model expressions.

Acknowledgements

J. Vancoillie gratefully acknowledges a Ph. D. fellowship (FWO09/ASP/030) and a travel grant for a long stay abroad (V407312N) of the Research Foundation - Flanders.

References

References

- [1] J. Vancoillie, J. Demuynck, L. Sileghem, M. Van De Ginste, S. Verhelst, L. Brabant, L. Van Hoorebeke, The potential of methanol as a fuel for flex-fuel and dedicated spark-ignition engines, *Applied Energy* 102 (2013) 140–149.
- [2] M. Specht, A. Bandi, Renewable carbon-based transportation fuels, Vol. 3C of Renewable Energy, Springer Berlin Heidelberg, Berlin, 2006.
- [3] R. Pearson, J. Turner, A. Peck, Gasoline-ethanol-methanol tri-fuel vehicle development and its role in expediting sustainable organic fuels for transport, in: IMechE Low Carbon Vehicles Conference, London, UK, 2009, pp. 1–21.
- [4] G. Olah, A. Goeppert, G. Prakash, Beyond Oil and Gas: the Methanol Economy., Wiley-VCH Verlag GmbH & Co.KGAA, Weinheim, Germany, 2006.
- [5] J. Vancoillie, M. Christensen, E. J. K. Nilsson, S. Verhelst, A. A. Konnov, Temperature dependence of the laminar burning velocity of methanol flames, *Energy & Fuels* 26 (3) (2012) 1557–1564.
- [6] J. Vancoillie, M. Christensen, E. J. K. Nilsson, S. Verhelst, A. A. Konnov, The effects of dilution with nitrogen and steam on the laminar burning velocity of methanol at room and elevated temperatures, *Fuel* 105 (2013) 732–738.
- [7] J. Vancoillie, S. Verhelst, J. Demuynck, Laminar burning velocity correlations for methanol-air and ethanol-air mixtures valid at SI engine conditions, SAE International, SAE paper no. 2011-01-0846 (2011).
- [8] J. Vancoillie, G. Sharpe, M. Lawes, S. Verhelst, Laminar burning velocities and markstein lengths of methanol-air mixtures at pressures up to 1.0 mpa, submitted to *Fuel* (2014).
- [9] M. Lawes, M. P. Ormsby, C. G. W. Sheppard, R. Woolley, The turbulent burning velocity of iso-octane/air mixtures, *Combustion and Flame* 159 (5) (2012) 1949–1959.
- [10] D. Bradley, M. Lawes, M. S. Mansour, Explosion bomb measurements of ethanol-air laminar gaseous flame characteristics at pressures up to 1.4 MPa, *Combustion and Flame* 156 (7) (2009) 1462–1470.
- [11] D. Bradley, R. A. Hicks, M. Lawes, C. G. W. Sheppard, R. Woolley, The measurement of laminar burning velocity and markstein numbers for iso-octane-air and iso-octane-n-heptane-air mixtures at elevated temperatures and pressures in an explosion bomb, *Combustion and Flame* 115 (1-2) (1998) 126–144.

- 460 [12] S. Verhelst, R. Sierens, A quasi-dimensional model for the power cycle of a hydrogen-fuelled ICE, *International Journal of Hydrogen Energy* 32 (15) (2007) 3545–3554.
- [13] M. S. Mansour, Fundamental study of premixed combustion rates at elevated pressure and temperature, Ph.D. thesis, University of Leeds (2010).
- 465 [14] S. Y. Liao, D. M. Jiang, Z. H. Huang, W. D. Shen, C. Yuan, Q. Cheng, Laminar burning velocities for mixtures of methanol and air at elevated temperatures, *Energy Conversion and Management* 48 (3) (2007) 857–863.
- [15] J. F. Driscoll, Turbulent premixed combustion: Flamelet structure and its effect on turbulent burning velocities, *Progress in Energy and Combustion Science* 34 (1) (2008) 91–134.
- 470 [16] D. Bradley, M. Lawes, M. S. Mansour, Correlation of turbulent burning velocities of ethanol-air, measured in a fan-stirred bomb up to 1.2 MPa, *Combustion and Flame* 158 (1) (2010) 123–138.
- [17] D. Bradley, M. Z. Haq, R. A. Hicks, T. Kitagawa, M. Lawes, C. G. W. Sheppard, R. Woolley, Turbulent burning velocity, burned gas distribution, and associated flame surface definition, *Combustion and Flame* 133 (4) (2003) 415–430.
- 475 [18] S. Verhelst, R. Woolley, M. Lawes, R. Sierens, Laminar and unstable burning velocities and markstein lengths of hydrogen-air mixtures at engine-like conditions, *Proceedings of the Combustion Institute* 30 (2005) 209–216.
- [19] S. Verhelst, A study of the combustion in hydrogen-fuelled internal combustion engines., Ph.D. thesis, Ghent University, doi: dx.doi.org/1854/3378 (2005).
- 480 [20] A. N. Lipatnikov, J. Chomiak, Molecular transport effects on turbulent flame propagation and structure, *Progress in Energy and Combustion Science* 31 (1) (2005) 1–73.
- [21] M. Lawes, M. P. Ormsby, C. G. W. Sheppard, R. Woolley, Variation of turbulent burning rate of methane, methanol, and iso-octane air mixtures with equivalence ratio at elevated pressure, *Combustion Science and Technology* 177 (7) (2005) 1273 – 1289.
- 485 [22] C. Morley. GASEQ: a chemical equilibrium program for Windows [online] (2005) [cited July 10th 2012].
- 490 [23] A. N. Lipatnikov, J. Chomiak, Turbulent flame speed and thickness: phenomenology, evaluation, and application in multi-dimensional simulations, *Progress in Energy and Combustion Science* 28 (1) (2002) 1–74.
- [24] V. L. Zimont, Gas premixed combustion at high turbulence. turbulent flame closure combustion model, *Experimental Thermal and Fluid Science* 21 (1-3) (2000) 179–186.
- 495

- [25] N. Peters, *Turbulent Combustion*, Cambridge University Press, Cambridge, 2000.
- [26] S. Richard, S. Bougrine, G. Font, F.-A. Lafossas, F. L. Berr, On the reduction of a 3D CFD combustion model to build a physical 0D model for simulating heat release, knock and pollutants in SI engines, *Oil and Gas Science and Technology - Rev. IFP* 64 (3) (2009) 223–242.
- 500 [27] Y.-W. Chin, R. D. Matthews, S. P. Nichols, T. M. Kiehne, Use of fractal geometry to model turbulent combustion in SI engines, *Combustion Science and Technology* 86 (1) (1992) 1 – 30.
- [28] C.-M. Wu, C. E. Roberts, R. D. Matthews, M. J. Hall, Effects of engine speed on combustion in si engines: Comparisons of predictions of a fractal burning model with experimental data, SAE International, SAE paper no. 932714 (1993).
- 505 [29] A. Teraji, A. Gurupatham, Development of flame propagation model considering Lewis number effect for fast idle condition, SAE International, SAE paper no. 2011-01-1892 (2011).
- [30] W. Dai, G. C. Davis, M. J. Hall, R. D. Matthews, Diluents and lean mixture combustion modeling for si engines with a quasi-dimensional model, SAE International, SAE paper no. 952382 (1995).
- 510 [31] C. D. Rakopoulos, C. N. Michos, E. G. Giakoumis, Thermodynamic analysis of si engine operation on variable composition biogas-hydrogen blends using a quasi-dimensional, multi-zone combustion model, SAE International, SAE paper no. 2009-01-0931 (2010).
- 515 [32] A. R. Kerstein, A linear-eddy model of turbulent scalar transport and mixing, *Combustion Science and Technology* 60 (4-6) (1988) 391–421.
- [33] O. L. Gülder, Turbulent premixed flame propagation models for different combustion regimes, *Symposium (International) on Combustion* 23 (1) (1991) 743–750.
- 520 [34] R. G. Abdel-Gayed, D. Bradley, M. Lawes, Turbulent burning velocities: A general correlation in terms of straining rates, *Proceedings of the Royal Society of London. A. Mathematical and Physical Sciences* 414 (1847) (1987) 389–413.
- [35] F. Bozza, A. Gimelli, S. S. Merola, B. Vaglieco, Validation of a fractal combustion model through flame imaging, SAE International, SAE paper no. 2005-01-1120 (2005).
- 525 [36] F. Bozza, A. Gimelli, L. Strazzullo, E. Torella, C. Cascone, Steady-state and transient operation simulation of a downsized turbocharged SI engine, SAE International, SAE paper no. 2007-01-0381 (2007).
- [37] R. D. Matthews, M. J. Hall, W. Dai, G. C. Davis, Combustion modeling in SI engines with a peninsula-fractal combustion model, SAE International, SAE paper no. 960072 (1996).
- 530

- [38] S. P. R. Muppala, N. K. Aluri, F. Dinkelacker, A. Leipertz, Development of an algebraic reaction rate closure for the numerical calculation of turbulent premixed methane, ethylene, and propane/air flames for pressures up to 1.0 mpa, *Combustion and Flame* 140 (4) (2005) 257–266.
- [39] H. Kobayashi, Y. Kawabata, K. Maruta, Experimental study on general correlation of turbulent burning velocity at high pressure, *Symposium (International) on Combustion* 27 (1) (1998) 941–948.
- [40] H. Kolla, J. W. Rogerson, N. Swaminathan, Validation of a turbulent flame speed model across combustion regimes, *Combustion Science and Technology* 182 (3) (2010) 284 – 308.
- [41] A. Teraji, T. Tsuda, T. Noda, M. Kubo, T. Itoh, Development of a novel flame propagation model (UCFM: Universal coherent flamelet model) for SI engines and its application to knocking prediction, *SAE International*, SAE paper no. 2005-01-0199 (2005).
- [42] F. Charlette, C. Meneveau, D. Veynante, A power-law flame wrinkling model for les of premixed turbulent combustion. part i: Non-dynamic formulation and initial tests, *Combustion and Flame* 131 (1-2) (2002) 159–180.

Table 1: Measured conditions for turbulent methanol-air flames. Quenched flames are indicated by q . * denotes conditions that were measured less than 3 times

p	1 bar			5 bar		
T_u	358 K			358 K		
ϕ	u' (m/s)			u' (m/s)		
0.8	2*	4	6 q	2	-	-
1.0	2	4	6	2	4	6
1.2	2	4	6	2	4*	-
1.4	2	4	6	2	4	6
1.6	2*	-	-	-	-	-

Table 2: Laminar burning velocities and Lewis numbers for turbulent methanol-air flames

p	1 bar			5 bar		
T_u	358 K			358 K		
ϕ	u_l (m/s)	L_b (mm)	Le	u_l (m/s)	L_b (mm)	Le
0.8	0.319	+0.92	1.04	0.182	+0.41	1.04
1.0	0.496	+0.85	0.96	0.337	+0.05	0.96
1.2	0.588	+0.73	0.89	0.421	-0.13	0.89
1.4	0.591	+0.55	0.85	0.395	-0.26	0.85
1.6	0.503	+0.40	0.82	-	-	-

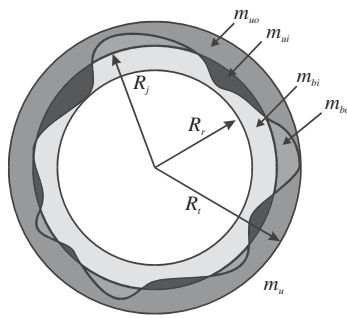


Figure 1: Masses of burned and unburned gas at a given instant during spherical explosive propagation. Mass of unburned gas inside sphere of radius R_j is m_{ui} , mass of burned gas outside it is m_{bo} . From [17]

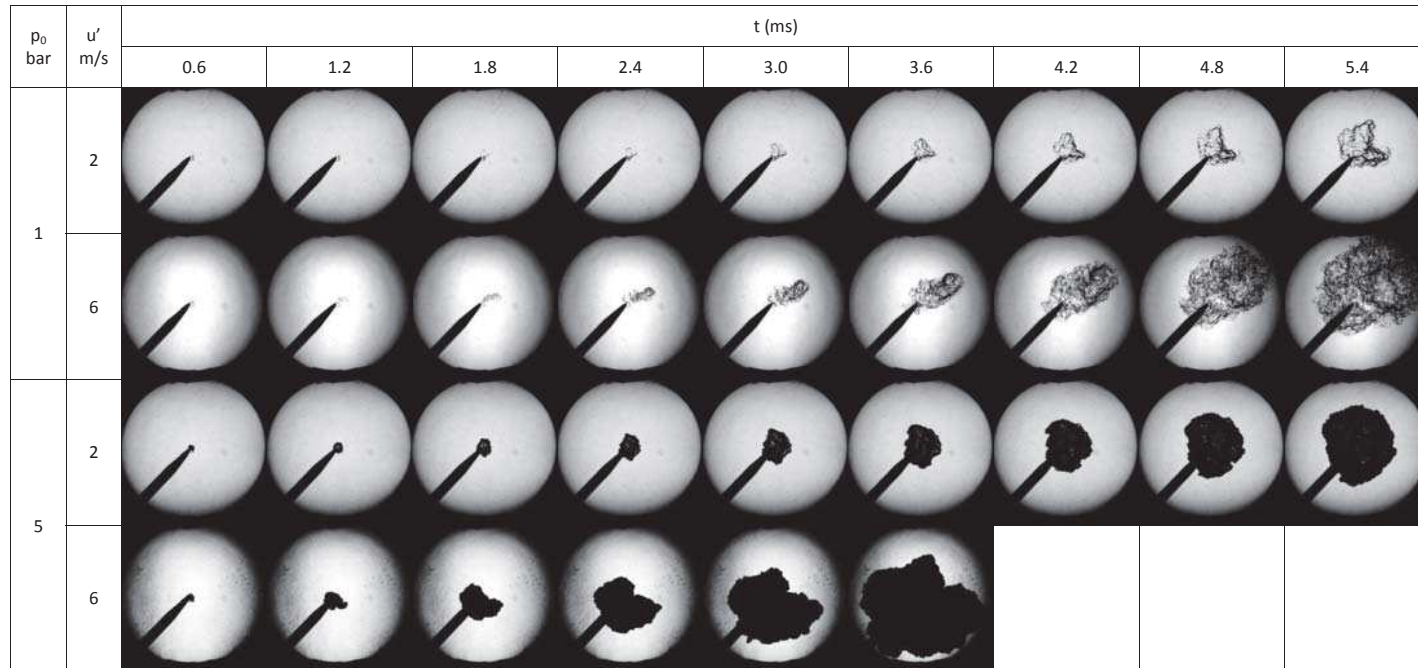


Figure 2: Turbulent flame propagation in a stoichiometric methanol-air mixture ($\phi = 1.0$) at an initial temperature of 358K and different initial pressures ($p = 1, 5$ bar) and rms turbulent velocities ($u' = 2, 6$ m/s).

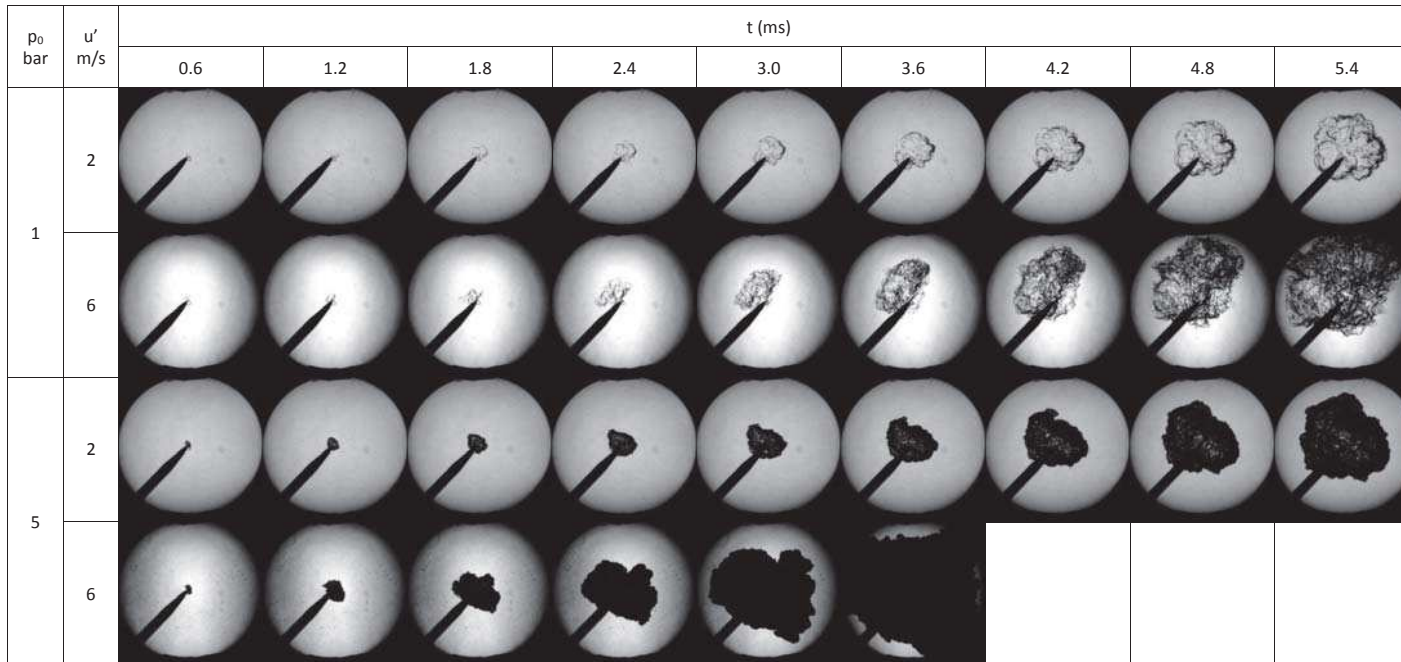


Figure 3: Turbulent flame propagation in a rich methanol-air mixture ($\phi = 1.4$) at an initial temperature of 358K and different initial pressures ($p = 1, 5$ bar) and rms turbulent velocities ($u' = 2, 6$ m/s).

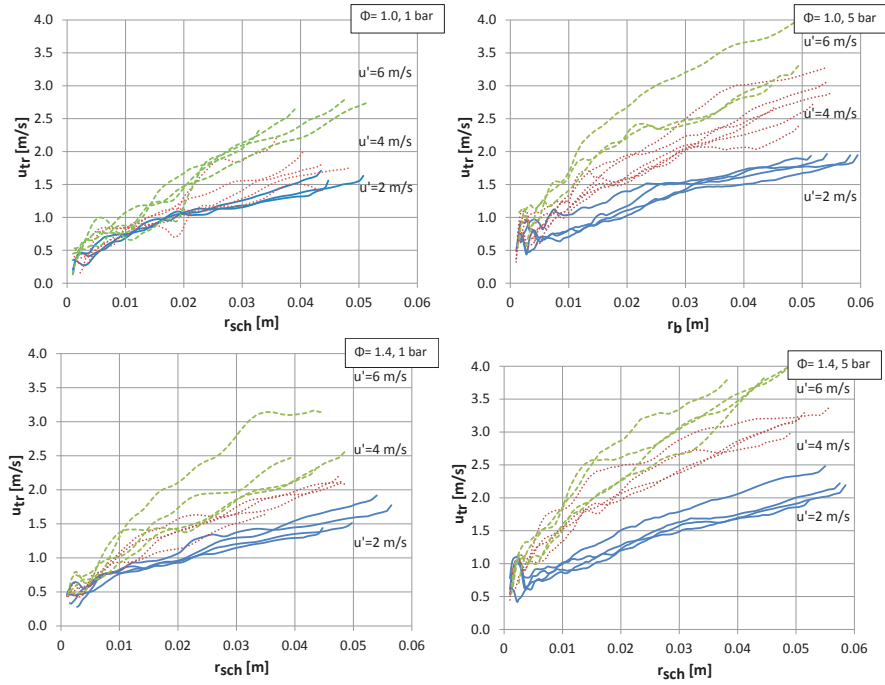


Figure 4: Burning velocity u_{tr} versus mean schlieren radius r_{sch} ($T_u=358$ K). The turbulent burning velocity increases with u' through more intense flame front wrinkling

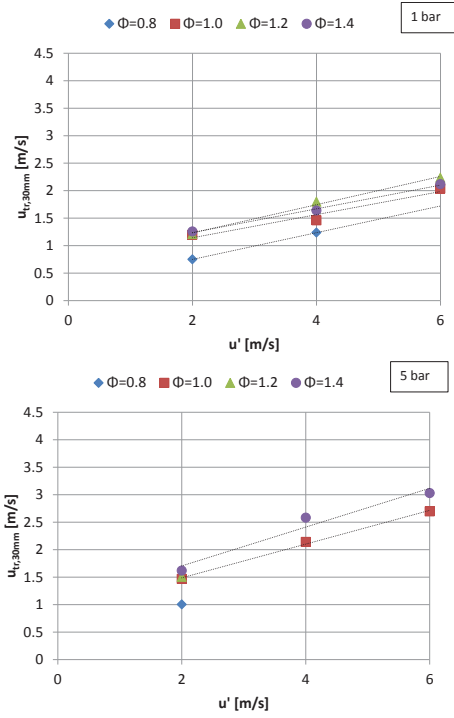


Figure 5: Burning velocity $u_{tr,30mm}$ versus u' ($T_u=358$ K)

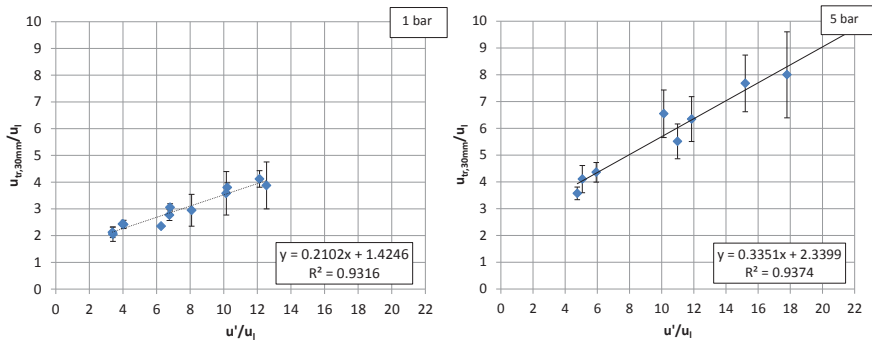


Figure 6: $u_{tr,30mm}/u_l$ versus u'/u_l ($T_u=358$ K)

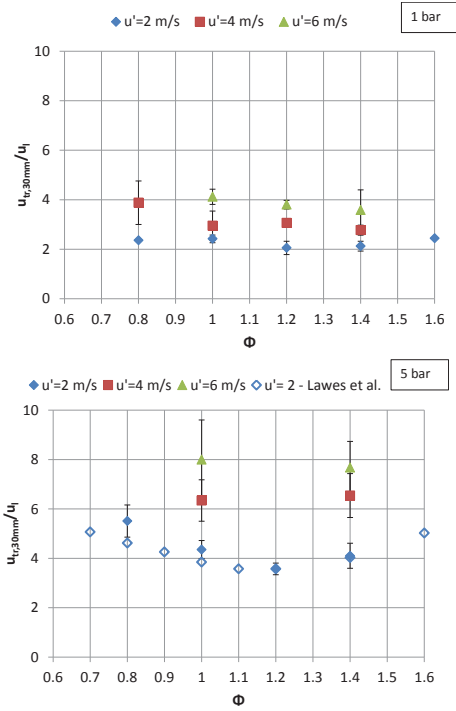


Figure 7: $u_{tr,30mm}/u_l$ versus ϕ ($T_u=358$ K)

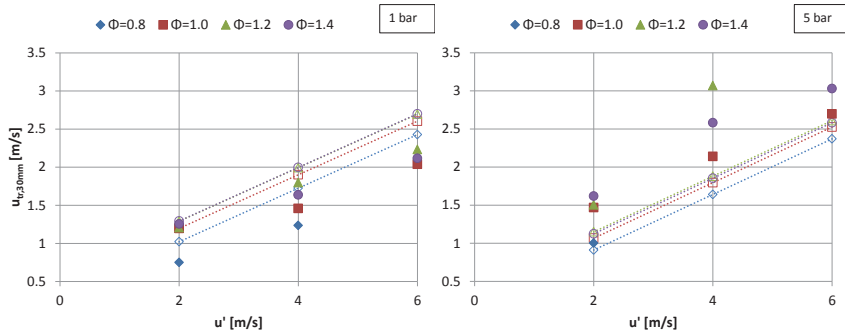


Figure 8: $u_{tr,30mm}$ vs. u' for the Damköhler model. Closed symbols - experiment, open symbols - model.

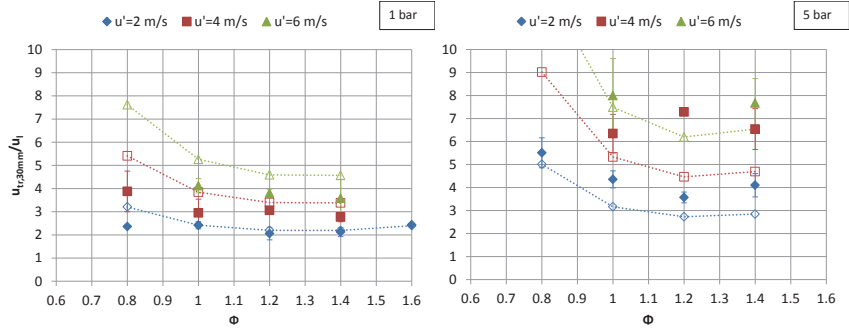


Figure 9: $u_{tr,30mm}/u_l$ vs. ϕ for the Damköhler model. Closed symbols - experiment, open symbols - model.

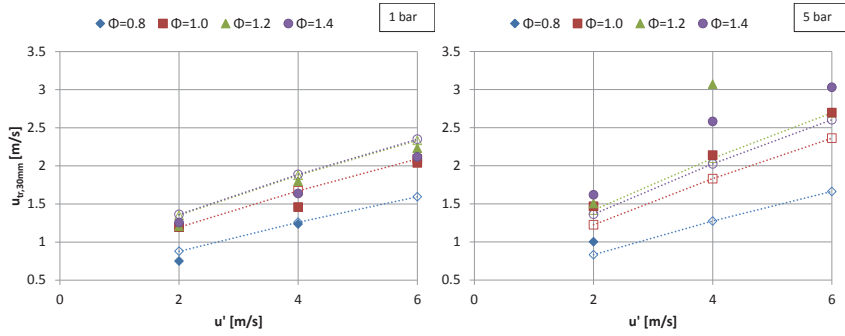


Figure 10: $u_{tr,30mm}$ vs. u' for the Gülder model. Closed symbols - experiment, open symbols - model.

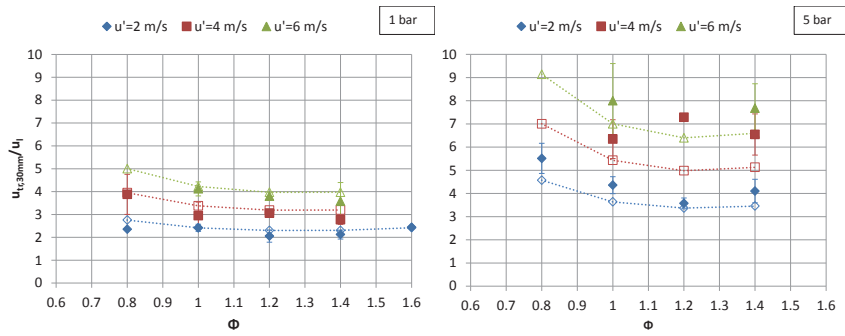


Figure 11: $u_{tr,30mm}/u_l$ vs. ϕ for the Gülder model. Closed symbols - experiment, open symbols - model.

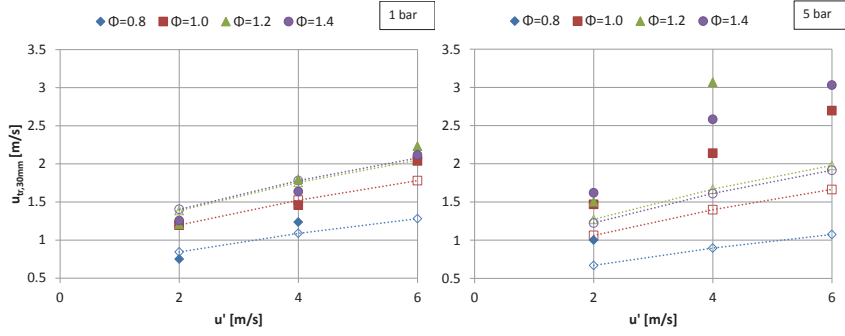


Figure 12: $u_{tr,30mm}$ vs. u' for the *KaLe* model of Bradley et al. Closed symbols - experiment, open symbols - model.

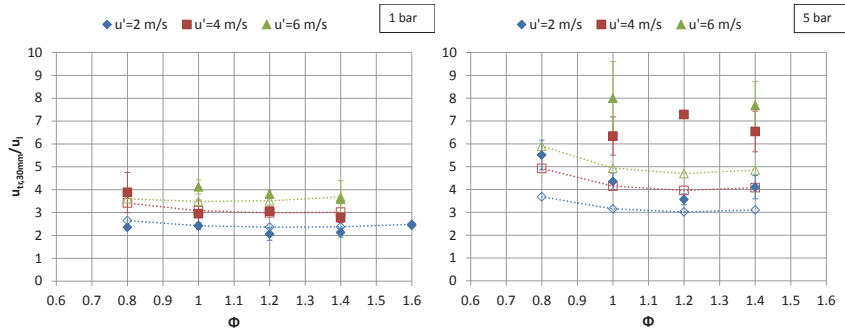


Figure 13: $u_{tr,30mm}/u_l$ vs. ϕ for the *KaLe* model of Bradley et al. Closed symbols - experiment, open symbols - model.

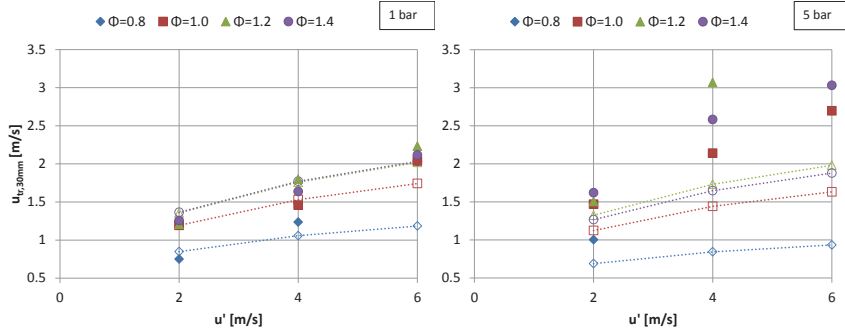


Figure 14: $u_{tr,30mm}$ vs. u' for the Fractals model. Closed symbols - experiment, open symbols - model.

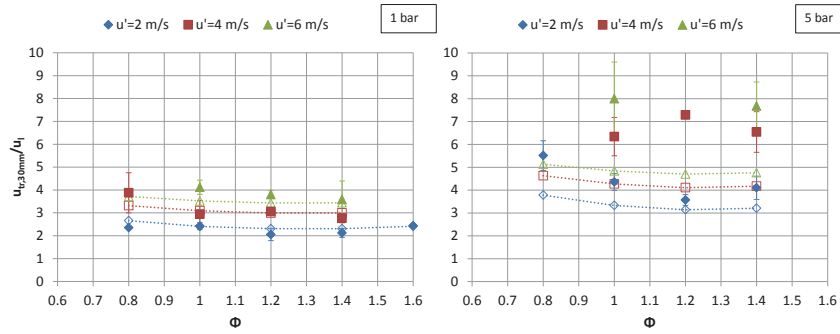


Figure 15: $u_{tr,30mm}/u_l$ vs. ϕ for the Fractals model. Closed symbols - experiment, open symbols - model.

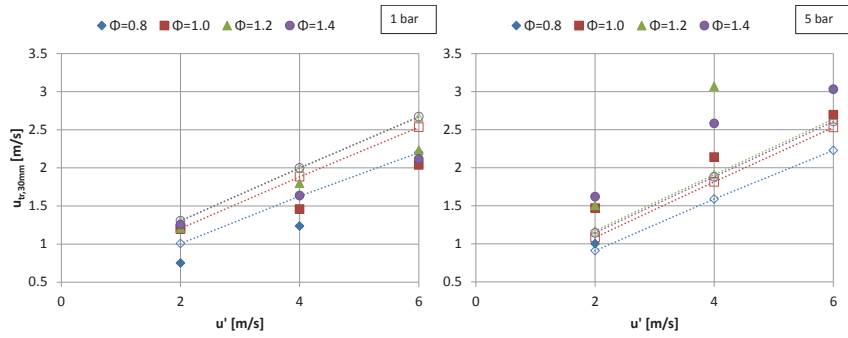


Figure 16: $u_{tr,30mm}$ vs. u' for the Peters model. Closed symbols - experiment, open symbols - model.

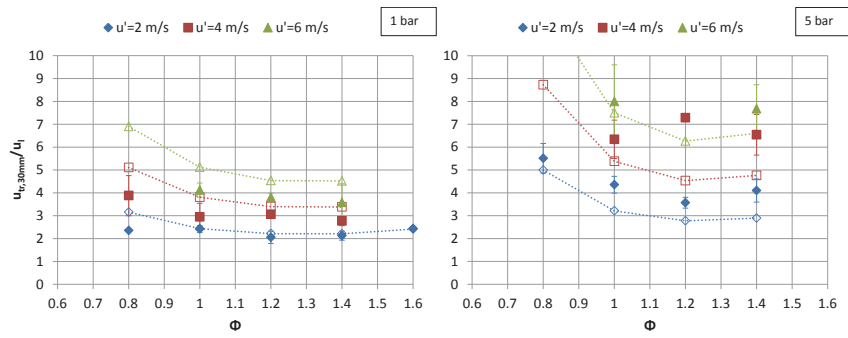


Figure 17: $u_{tr,30mm}/u_l$ vs. ϕ for the Peters model. Closed symbols - experiment, open symbols - model.

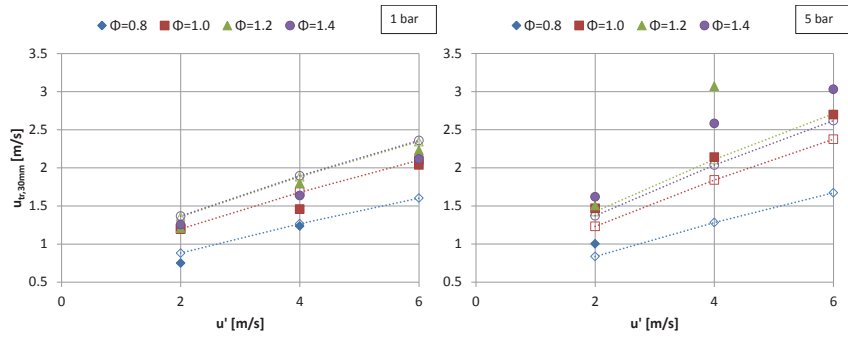


Figure 18: $u_{tr,30mm}$ vs. u' for the Zimont model. Closed symbols - experiment, open symbols - model.

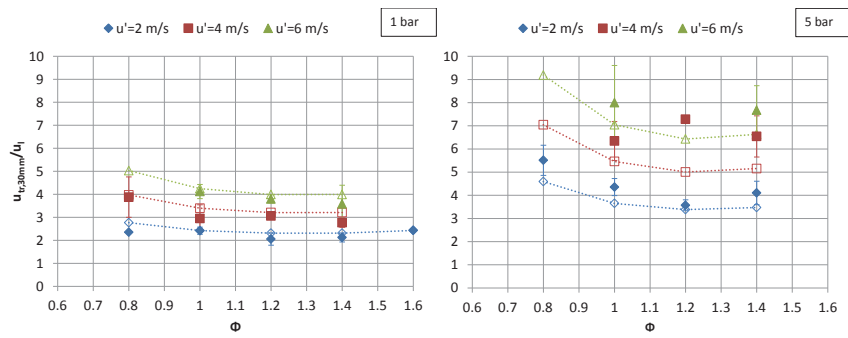


Figure 19: $u_{tr,30mm}/u_l$ vs. ϕ for the Zimont model. Closed symbols - experiment, open symbols - model.

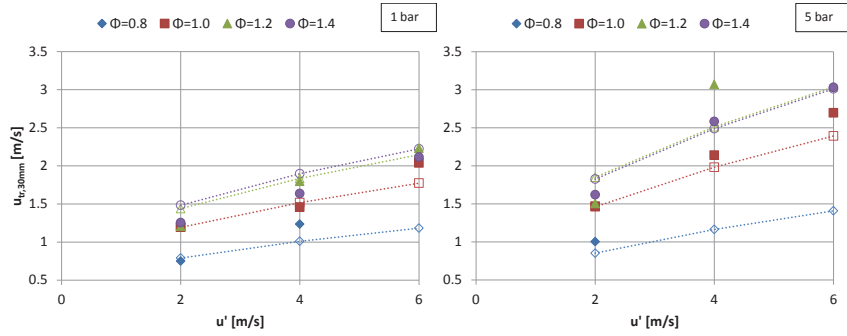


Figure 20: $u_{tr,30mm}$ vs. u' for the Dinkelacker model. Closed symbols - experiment, open symbols - model.

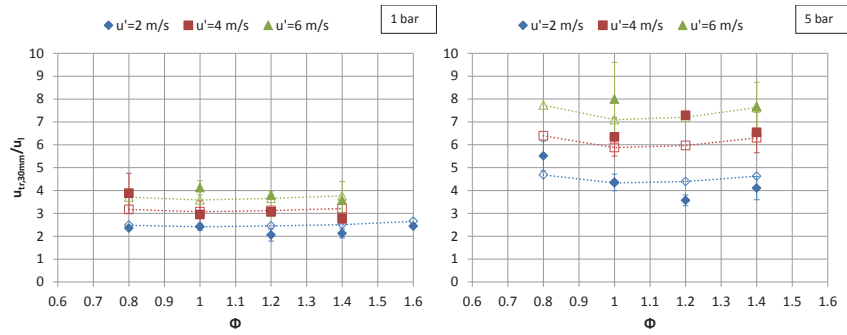


Figure 21: $u_{tr,30mm}/u_l$ vs. ϕ for the Dinkelacker model. Closed symbols - experiment, open symbols - model.

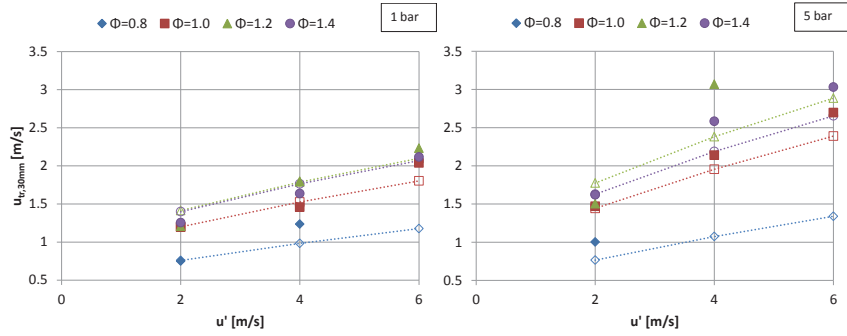


Figure 22: $u_{tr,30mm}$ vs. u' for the Kolla model. Closed symbols - experiment, open symbols - model.

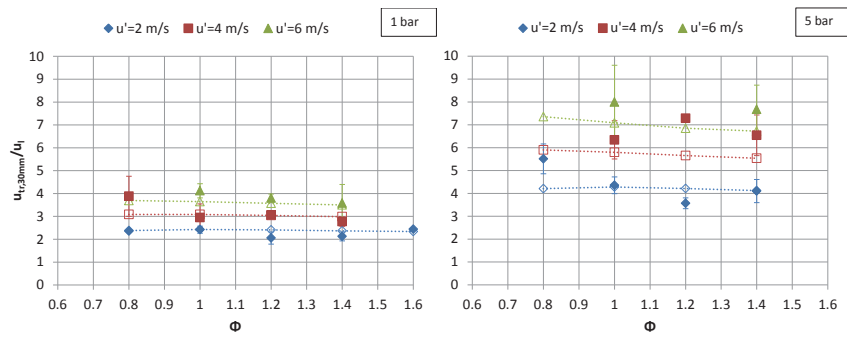


Figure 23: $u_{tr,30mm}/u_l$ vs. ϕ for the Kolla model. Closed symbols - experiment, open symbols - model.

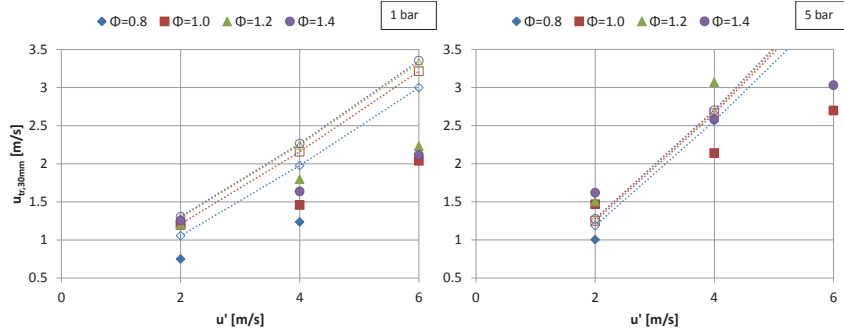


Figure 24: $u_{tr,30mm}$ vs. u' for the CFM with Γ according to Eqs. A.21 - A.26. Closed symbols - experiment, open symbols - model.

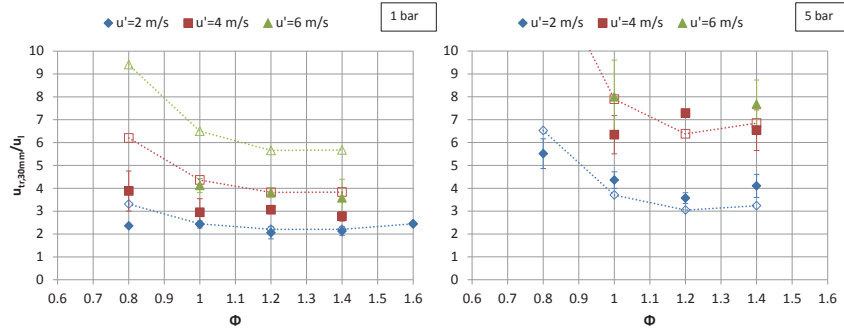


Figure 25: $u_{tr,30mm}/u_l$ vs. ϕ for the CFM with Γ according to Eqs. A.21 - A.26. Top - Methanol, bottom - ethanol. Closed symbols - experiment, open symbols - model.

550 Appendix A. Turbulent burning velocity models

Appendix A.1. Damköhler and derivatives

A large number of models assume the sole effect of turbulence to be flame front wrinkling leading to an increased flame area. Thus, the burning velocity ratio u_t/u_l is assumed to be equal to the flame surface area ratio A_t/A_l , where A_t is the wrinkled surface area and A_l is the mean, smooth flame surface area. Damköhler related this area ratio to the rms turbulent velocity divided by the laminar burning velocity:

$$\frac{A_t}{A_l} \sim \frac{u'}{u_l} \Rightarrow u_t \sim u' \quad (\text{A.1})$$

This expression is claimed to be valid for large u'/u_l . In many engine models the expression is changed to $u_t \sim u' + u_l$ to recover the laminar burning velocity when $u' \rightarrow 0$.

560 *Appendix A.2. Gülder*

Gülder derived the following expression for u_t [33, 19]

$$u_t = u_l + 0.6u'^{0.5}u_l^{0.5}Re_t^{0.25} \quad (\text{A.2})$$

565 Gülder later plotted $u_t/u_l - 1$ versus $(u'/u_l)^{0.5}Re_t^{0.25}$, where $Re_t = u'\Lambda/\nu$, for a large experimental dataset obtained from different research groups and obtained good approximation of the data with Equation A.2. Note that a large part of this dataset did not take into account the effects of flame stretch and instabilities on the laminar burning velocity.

Appendix A.3. Bradley et al.

570 Bradley et al. collected all known experimental values of turbulent burning velocities and searched for correlations on a theoretical basis using dimensionless terms describing the data set [34]. They developed a correlation in terms of the Lewis number Le and the Karlovitz stretch factor Ka , representing the dimensionless flow field strain.

$$u_t/u' = 0.88(KaLe)^{-0.3} \quad (\text{A.3})$$

575 where Ka was taken as $Ka = 0.157(u'/u_l)^2Re_t^{-0.5}$. The dependence of u_t/u' on the product $KaLe$ originated from the consideration of the effect of flame stretch on u_t , starting from the linear relation between flame speed and flame stretch for the local laminar flame [11].

Appendix A.4. Fractal-based models

580 Starting from Gouldin's suggestion of using a fractal geometry to describe the self-similar wrinkling of the flame front by the turbulence spectrum, Matthews et al. developed the following expression for the area increase [27, 28].

$$\frac{A_t}{A_l} = \left(\frac{L_{max}}{L_{min}} \right)^{D_3-2} \quad (\text{A.4})$$

L_{max} and L_{min} are the outer and inner cut-off of the wrinkling, D_3 is the fractal dimension of the flame surface. The ratio L_{max}/L_{min} is mostly set to the ratio of maximum to minimum turbulent length scale Λ/η_K [27, 35, 36].

585 The fractal dimension D_3 is given by Equation A.5 and describes the balance between turbulent flame wrinkling and laminar flame smoothing through flame propagation.

$$D_3 = 2.35 \frac{u'}{u' + u_l} + 2.0 \frac{u_l}{u' + u_l} \quad (\text{A.5})$$

Some authors account for the effect of stretch on the local flame speed by using the stretched laminar burning velocity u_n in their u_t model. u_n is then derived using a stretch model [30, 37, 29].

$$u_t = u_n \left(\frac{L_{max}}{L_{min}} \right)^{D_3-2} \quad (\text{A.6})$$

590 *Appendix A.5. Peters*

Peters derived an expression for the flame surface area increase due to turbulence using the G equation framework [25]. Considering a regime of highly turbulent combustion, with a thin reaction zone but thickened preheat zone through small scale eddy penetration, he obtained the following expression for u_t :

$$u_t = u_l + u' \left\{ -\frac{a_4 b_3^2}{2b_1} Da + \left[\left(\frac{a_4 b_3^2}{2b_1} Da \right)^2 + a_4 b_3^2 Da \right]^{1/2} \right\} \quad (\text{A.7})$$

595 Peters suggests the following values: $a_4 = 0.78$, $b_1 = 2.0$ and $b_3 = 1.0$.

Appendix A.6. Zimont/Lipatnikov

For the turbulent burning velocity u_t , Zimont suggested the following model:

$$u_t = Au' Da^{1/4} = Au' \left(\frac{\Lambda}{u' \tau_l} \right)^{1/4} \quad (\text{A.8})$$

600 where τ_l is a chemical time scale and A is a calibration constant with a suggested value of 0.5. The chemical time scale is based on the laminar flame thickness, using the molecular heat diffusivity D_t as the relevant diffusivity: $\tau_l = \delta_l / u_l = D_t / u_l^2$. The extended model of Lipatnikov and Chomiak with this expression for u_t has been validated against measurements in fan-stirred bombs, SI engines and several experimental databases [23].

Appendix A.7. Dinkelacker et al.

605 Dinkelacker et al. developed a turbulent burning velocity correlation based on a dataset measured by Kobayashi et al. of over 100 cone angles of bunsen flames for lean methane-, ethylene- and propane-air flames at operating pressures between 0.1-1.0 MPa [38]. They computationally estimated the flame cone angle using a 3D RANS simulation employing the common turbulent gradient diffusion approach for turbulent scalar transport and the following expression for the mean reaction source term \bar{w}_c :

$$\bar{w}_c = \rho_u u_l I_0 \Sigma \quad (\text{A.9})$$

The flame surface density Σ and stretch factor I_0 were directly modeled by an empirical expression for A_t/A_l :

$$\frac{A_t}{A_l} = \frac{u_t}{u_l} = 1 + a Re_t^{0.25} \left(\frac{u'}{u_l} \right)^b \left(\frac{p}{p_0} \right)^c \quad (\text{A.10})$$

615 The form of this correlation was inspired by the correlation of Gülder (see Appendix A.2) and earlier work by Kobayashi et al. on the pressure dependence of turbulent burning velocity [39]. The constant a and exponents b and c were determined by numerical optimization comparing the experimental and calculated flame cone angles.

Exponents b and c were found to be universal across fuels, whereas a was fuel dependent. A good correlation was found between a and the Lewis number of the fuel-air mixture. The final correlation was:

$$\frac{u_t}{u_l} = 1 + \frac{0.46}{Le} Re_t^{0.25} \left(\frac{u'}{u_l} \right)^{0.3} \left(\frac{p}{p_0} \right)^{0.2} \quad (\text{A.11})$$

620 Inclusion of the Lewis number is reported to represent the effect of instabilities at low turbulence and that of stretch of the mainly positively curved leading edge of the flame brush.

Appendix A.8. Kolla et al.

625 Kolla et al. recently developed an expression for the leading edge turbulent burning velocity u_t using the Kolmogorov-Petrovskii-Piskunov (KPP) analysis [23, 40] in combination with their scalar dissipation rate model to close the mean reaction rate model:

$$\frac{u_t}{u_l} = \left\{ \frac{18C_\mu}{(2C_m - 1)\beta'} \left[[2K_c^* - \tau C_4] \left(\frac{u'\Lambda}{u_l \delta_l} \right) + \frac{2C_3}{3} \left(\frac{u'}{u_l} \right)^2 \right] \right\}^{1/2} \quad (\text{A.12})$$

The model constants in Equation A.12 were obtained using DNS data.

- C_m is typically 0.7
- 630 • K_c^* is related to the dilatation rate and is given by $K_c^* \approx 0.85\tau$ where τ is a heat release parameter given by $\tau = (T_{ad} - T_u)/T_u$
- β' represents the flamelet curvature contribution and its value is 6.7
- C_3 and C_4 represent turbulence-scalar interaction effects and depend on the Karlovitz number Ka

$$Ka = \left(\frac{\nu_u}{u_l \eta_K} \right)^2 = \left([2(1 + \tau)^{0.7}]^{-1} \left(\frac{u'}{u_l} \right)^3 \left(\frac{\delta_l}{\Lambda} \right) \right)^{0.5} \quad (\text{A.13})$$

$$C_3 = \frac{1.5 \sqrt{Ka}}{1 + \sqrt{Ka}} \quad (\text{A.14})$$

$$C_4 = 1.1(1 + Ka)^{-0.4} \quad (\text{A.15})$$

635 Appendix A.9. Coherent Flame Model

As stated by Driscoll, turbulent flame wrinkling is a geometry dependent process and has a memory of upstream locations [15]. Coherent Flame Models (CFM) are a class of models that implement this observation by solving a transport equation for the temporal and spatial evolution of the flame surface density Σ [15, 26, 41]. The general form of this equation is usually as follows:

$$\frac{d\Sigma}{dt} + \frac{\partial u_i \Sigma}{\partial x_i} = \frac{\partial}{\partial x_i} \left(\frac{\nu_t}{\sigma_c} \frac{\partial \Sigma}{\partial x_i} \right) + S - M - Q \quad (\text{A.16})$$

The two terms on the left hand side represent the convection of wrinkledness to downstream locations. The first term on the right hand side simulates the spreading of the flame brush due to turbulent diffusion. The three other terms on the right hand side respectively represent the source term for flame surface density, the mean merging rate of flame surface and the mean flame front quenching rate. Many models have been proposed for these three terms [41, 15]. The model is an analytical formulation of a turbulent flame consisting of coherent laminar flame elements (flamelets), where by coherent, it is implied that a local laminar flamelet retains its identity although it is severely distorted and strained by the turbulent motions.

Richard et al. have recently reduced their 3D CFM model to a formulation that is compatible with quasi-dimensional engine modeling [26]. The mass burning rate was given by:

$$\dot{m}_b = \rho_u u_l A_l \Sigma \quad (\text{A.17})$$

where A_l is the mean, smooth flame front surface and Σ is the flame surface density, of which the temporal evolution is described by the following balance equation.

$$\frac{1}{\Sigma} \frac{d\Sigma}{dt} = \Gamma(u'/u_l, \Lambda/\delta_l) \frac{u'}{\Lambda} \left(\frac{\Sigma_{eq} - \Sigma}{\Sigma_{eq} - 1} \right) - \frac{2}{r_{bg}} (1 + \tau)(\Sigma - 1)u_l \quad (\text{A.18})$$

where $\tau = \rho_u/\rho_b$, $r_{bg} = (3V_b/4\pi)^{1/3}$ is the burnt gas mean radius and the laminar flame thickness δ_l is computed according to $\delta_l = \nu/u_l$. The stretch efficiency function Γ measures the efficiency of turbulence motions to wrinkle the flame front. The first term on the right hand side represents the flame strain caused by all turbulent structures, while the second simulates the effect of thermal expansion, which limits the flame front wrinkling by imposing positive curvature on the flame front [26]. Σ_{eq} is the value of Σ when equilibrium is reached between turbulence and flame front wrinkling. It is given by:

$$\Sigma_{eq} = 1 + \frac{2}{u_l} \sqrt{\frac{C\Gamma u'^2}{1 - C^*/(1 + \tau)}} \quad (\text{A.19})$$

Where proposed values for the constants are $C^*=0.5$ and $C=0.12$. Richard et al. [26] report that the use of a balance equation for Σ improves the transition from laminar to turbulent combustion compared to fractal modeling approaches such as that by Bozza et al. [35]. Here, this equation is solved between spark time and the experimental time for which the burned gas radius $r_b=0.03$ m (t_{30mm}), with the assumption of constant u' and a quadratic evolution of r_b .

$$r_b(t) = \frac{0.03}{t_{30mm}^2} \cdot t^2 \quad (\text{A.20})$$

The stretch efficiency function Γ is mainly a function of the integral length scale and the laminar flame thickness, and is nearly independent from the rms turbulent burning velocity u' [15]. Charlette et al. obtained an expression for $\Gamma(u'/u_l, \Lambda/\delta_l, Re_t)$ from

spectral analysis of DNS simulation of single vortex-flame interactions [42]:

$$\Gamma = [(f_u^{-a} + f_\Lambda^{-a})^{-1/a}]^{-b} + f_{Re}^{-b}]^{-1/b} \quad (\text{A.21})$$

$$f_u = 4 \left(\frac{27C_k}{110} \right)^{1/2} \left(\frac{18C_k}{55} \right) \left(\frac{u'}{u_i} \right)^2 \quad (\text{A.22})$$

$$f_\Lambda = \left[\frac{27C_k \Pi^{4/3}}{110} \cdot \left(\left(\frac{\Lambda}{\delta_l} \right)^{4/3} - 1 \right) \right]^{1/2} \quad (\text{A.23})$$

$$f_{Re} = \left[\frac{9}{55} \exp \left[-\frac{3}{2} C_k \Pi^{4/3} Re_i^{-1} \right] \right]^{1/2} \cdot Re_i^{1/2} \quad (\text{A.24})$$

$$a = 0.60 + 0.20 \exp[-0.1(u'/u_i)] - 0.20 \exp[-0.01(\Lambda/\delta_l)] \quad (\text{A.25})$$

$$b = 1.4 \quad (\text{A.26})$$